

# **The application of Trefftz-FLAME to electromagnetic wave problems**

By Helder Fleury Pinheiro

BEng, MEng, DrEng (Electrical)

Department of Electrical Engineering

McGill University

Montreal, Canada

A thesis submitted to the Faculty of Graduate Studies and Research

in partial fulfillment of the requirements for the degree of

Doctor of Philosophy

18 August, 2008

© Helder Fleury Pinheiro, 2008



Library and Archives  
Canada

Published Heritage  
Branch

395 Wellington Street  
Ottawa ON K1A 0N4  
Canada

Bibliothèque et  
Archives Canada

Direction du  
Patrimoine de l'édition

395, rue Wellington  
Ottawa ON K1A 0N4  
Canada

*Your file* *Votre référence*  
ISBN: 978-0-494-66570-1  
*Our file* *Notre référence*  
ISBN: 978-0-494-66570-1

**NOTICE:**

The author has granted a non-exclusive license allowing Library and Archives Canada to reproduce, publish, archive, preserve, conserve, communicate to the public by telecommunication or on the Internet, loan, distribute and sell theses worldwide, for commercial or non-commercial purposes, in microform, paper, electronic and/or any other formats.

The author retains copyright ownership and moral rights in this thesis. Neither the thesis nor substantial extracts from it may be printed or otherwise reproduced without the author's permission.

---

In compliance with the Canadian Privacy Act some supporting forms may have been removed from this thesis.

While these forms may be included in the document page count, their removal does not represent any loss of content from the thesis.

**AVIS:**

L'auteur a accordé une licence non exclusive permettant à la Bibliothèque et Archives Canada de reproduire, publier, archiver, sauvegarder, conserver, transmettre au public par télécommunication ou par l'Internet, prêter, distribuer et vendre des thèses partout dans le monde, à des fins commerciales ou autres, sur support microforme, papier, électronique et/ou autres formats.

L'auteur conserve la propriété du droit d'auteur et des droits moraux qui protègent cette thèse. Ni la thèse ni des extraits substantiels de celle-ci ne doivent être imprimés ou autrement reproduits sans son autorisation.

---

Conformément à la loi canadienne sur la protection de la vie privée, quelques formulaires secondaires ont été enlevés de cette thèse.

Bien que ces formulaires aient inclus dans la pagination, il n'y aura aucun contenu manquant.

  
**Canada**

## Abstract

Numerical analysis of the electromagnetic fields in large, complex structures is very challenging due to the high computational overhead. Recently, it has been shown that a new method called Trefftz-FLAME (*Flexible Local Approximation MEthod*) is suitable for problems where there exist a large number of similar structures.

This thesis develops Trefftz-FLAME in two areas. First, a novel 2D Trefftz-FLAME method incorporates the modal analysis and port boundary condition that are essential to an accurate calculation of reflection and transmission coefficients for photonic crystal devices. The new technique outperforms existing methods in both accuracy and computational cost.

The second area pertains to the 3D, vector problem of electromagnetic wave scattering by aggregates of identical dielectric particles. A methodology for the development of local basis functions is introduced, applicable to particles of any shape and composition. Boundary conditions on the surface of the finite FLAME domain are described, capable of representing the incident wave and absorbing the outgoing radiation. A series of problems involving dielectric spheres is solved to validate the new method. Comparison with exact solutions is possible in some cases and shows that the method is able to produce accurate near-field results even when the computational grid spacing is equal to the radius of the spheres.

## Résumé

L'analyse numérique des champs électromagnétiques appliquée aux grandes structures complexes est un défi en raison de la forte demande des ressources computationnelles. Récemment, il a été démontré qu'une nouvelle méthode appelée Trefftz-FLAME (*Flexible Local Approximation MEthod*) est idéale pour les problèmes où il y a un grand nombre de structures similaires. Cette thèse développe Trefftz-FLAME en deux parties. D'abord, une nouvelle méthode 2D Trefftz-FLAMME a été établie par l'incorporation de la condition de port reposant sur l'analyse modale essentielle à un calcul précis des coefficients de réflexion et de transmission pour les dispositifs à cristaux photoniques. La nouvelle technique surpasse les méthodes existantes en termes de précision et du coût de calcul.

Dans la deuxième partie, une nouvelle méthode tridimensionnelle et vectorielle est proposée pour résoudre le problème de la diffusion d'ondes électromagnétiques par des agrégats de particules identiques entrant dans la composition de matériaux diélectriques. Une méthodologie pour le développement de fonctions de base local est ainsi créée, applicable à toute forme de particules et de composition. De plus, les conditions des frontières pour FLAME sont décrites, capables de représenter l'onde incidente et absorbant le rayonnement sortant. Une série de problèmes impliquant des sphères diélectriques est résolue afin de valider la nouvelle méthode. La comparaison avec des solutions exactes est possible dans certains cas et cela montre aussi que la méthode est en mesure de produire des résultats précis pour le champ proche même si le pas de discrétisation est égal au rayon des sphères.

## **Acknowledgements**

I would like to thank my supervisor Professor Jon P. Webb for his close supervision, support and valuable insights throughout this research.

Further, I would like to thank my colleagues and friends at McGill.

Finally, McGill University is also gratefully acknowledged

## Table of Contents

<b>Abstract</b> .....	i
<b>Résumé</b> .....	ii
<b>Acknowledgements</b> .....	iii
<b>Table of contents</b> .....	iv
<b>Chapter 1 - Introduction</b> .....	1
1.1 Birth of Trefftz - FLAME.....	2
1.2 Outline of Trefftz - FLAME formulation.....	3
1.3 Merits and drawbacks of Trefftz - FLAME.....	3
1.4 Motivation, goals and thesis contribution.....	4
1.4.1 Photonic crystal devices.....	5
1.4.2 Aggregate of identical dielectric particles.....	5
1.5 Outline of the thesis.....	7
<b>Chapter 2 - The Trefftz - FLAME method</b> .....	8
2.1 Basic formulation.....	8
<b>Chapter 3 - Application of Trefftz - FLAME for Modeling Photonic devices</b> .....	12
3.1 Problem definition.....	12
3.2 Basis functions.....	14
3.3 Plane waves basis functions.....	15
3.4 Approximate absorbing boundary conditions (ABC).....	17
3.5 Cylindrical harmonic basis functions.....	18
3.6 Applying the Trefftz - FLAME method.....	19
3.7 Trefftz - FLAME for the waveguide mode calculation.....	20
3.8 The Port Boundary Condition.....	22

3.9 Scattering Analysis.....	23
3.10 Numerical results.....	23
3.11 Discussions.....	29
<b>Chapter 4 - Vectorial 3D Trefftz - FLAME for the scattering analysis of dielectric particles.....</b>	<b>31</b>
4.1 Statement of the problem.....	32
4.2 Applying the Trefftz-FLAME method.....	33
4.2.1 Computational Molecule.....	33
4.2.2 Basis Functions.....	34
4.2.2.1 STEP 1: the set of incident waves.....	36
4.2.2.2 STEP 2: Finding the scattered field.....	39
4.2.2.3 STEP 3: Mapping to the global coordinates.....	40
4.2.3 Basis functions when there is no scatterer.....	41
4.3 ABC computational molecule.....	42
4.4 Setting the excitation - plane - ABC.....	44
4.5 Numerical experiments.....	44
4.5.1 Single dielectric sphere.....	44
4.5.2 Two spheres.....	46
4.5.3 A planar distribution of 10 dielectric spheres.....	48
4.6 Conclusions.....	50
<b>Chapter 5 - Conclusions.....</b>	<b>51</b>
5.1 Original contributions.....	52
5.2 Future trends.....	52
<b>Appendix A - Basis functions for spherical dielectric scatterer.....</b>	<b>54</b>
<b>Appendix B - Far field calculations.....</b>	<b>57</b>
<b>References.....</b>	<b>60</b>

# Chapter 1

## Introduction

Nowadays there are many well-established numerical techniques for electromagnetic analysis, e.g. Finite Differences in the Time Domain (FDTD) [1-3], the Finite Element Method (FEM) [4] and the Boundary Integral Method. Yet still the electromagnetic analysis of a large scale problem, especially in three dimensions, is very challenging. These techniques require tremendous amounts of computer memory and CPU time for large problems.

New techniques have been proposed for one increasingly important class of large scale problem: the electromagnetic behaviour of many identical structures. The most studied case is that of an infinite periodic array [5-8], which can be solved by considering just a unit cell. More challenging are cases where the array is finite, or defective, or there is no array at all, but just an arbitrary arrangement of identical bodies. A FEM Domain Decomposition Method has been proved very efficient for such problems and has been used in the analysis of three dimensional (3-D) finite electromagnetic band gap structures [9]. A very promising alternative known by the acronym FLAME (Flexible Local Approximation Method) was recently developed [10]. The basic FLAME approach builds variational-difference schemes with arbitrary local approximating basis functions. Later the Trefftz version of FLAME was proposed, a generalized finite difference method that replaces the Taylor polynomials of classical FDM with local basis functions that satisfy exactly the governing differential equation [11].

In 1926 E. Trefftz published a paper about a variational formulation as a counterpart for the Rayleigh-Ritz method for solving boundary value problem. The Trefftz idea was to use a linear combination of trial functions which satisfied *a priori* the governing differential equation [12]. Moreover, this pioneer paper incorporated the idea of partitions of the region of interest (subdomains), and the use of trial functions in each one of the regions. Half a century later, researchers picked up again the ideas of Trefftz and combined them with both Finite Element and Boundary Element methods. As a matter of fact, Trefftz concepts have led to a class of numerical method called Trefftz-

based methods [13] which have been used in many applications involving the Poisson, Laplace, Helmholtz, Navier and biharmonic equations [14-16]. Trefftz-based methods have been proved for solving problems in elasticity as well as to elasto-plasticity, heat transfer, acoustics, structural mechanics, plates, shells [17-20], and electromagnetics [21, 22]. Indeed, a wealth of literature on the subject has appeared in recent years and an arsenal of shape functions or complete functions sets called T-sets [23] which are locally exact solutions have been developed, such as cylindrical and spherical harmonics to the Helmholtz equation [24], functions that describe the behaviour of potential and fields near sharp edges [25] and functions that represent a finite number of plane waves of the Maxwell's equations [26].

### **1.1 Birth of Trefftz-FLAME**

Further research led to different techniques by using functions in the sense of Trefftz. Actually, many scattered contributions to the Trefftz method can be found in the literature. For instance, Sakai presented a technique called LENS (locally exact numerical scheme) for solving the transport equation with source terms. LENS is based on the locally exact numerical differencing [27]. Regarding the electromagnetic applications, special mention is made here of the work by Hadley [28-30]. He presented several papers showing the use of a special high-order Finite Difference scheme for analysis of waveguides. He incorporated Bessel functions, satisfying the two-dimensional Helmholtz equation, upon a nine-point stencil used to derive the standard finite-difference equations. He examined the behavior of electric and magnetic fields in waveguides, cylindrical cavity, vertical-cavity laser structure and fields in the vicinity of a dielectric corner. Highly accurate results were obtained with a modest increase in numerical effort in comparison with standard FDM. The name "Trefftz" indicates that the trial or basis functions satisfy all governing differential equations. Taking this point of view one could classify Hadley's formulation as a Trefftz-Finite Difference Method. A few years later, Tsukerman provided a more general and systematic way of developing differences schemes that can contain any desired approximation of the solution including functions that satisfy *a priori* the governing differential problem equations. This new procedure

gave birth to Trefftz-FLAME [31-33]. It has proved successful in a variety of applications, e.g. electrostatic or magnetostatic problems with cylindrical or spherical particle, multiparticle interactions [34-39], scattering of electromagnetic waves from an infinite dielectric cylinder, wave computations in photonic crystal waveguides [40] and Photonic Band Gap structures [41], and wave refraction in negative index materials [42].

## 1.2 Outline of Trefftz-FLAME formulation

The crucial ingredient of the Trefftz approach is the design of basis functions which are linearly independent and satisfy, *a priori*, the governing differential equation within a computational molecule (Finite Difference stencil). Once this is done, one or more equations can be developed that relate the values at the nodes of the molecule and are the discrete representation of the differential equation within the molecule. Finally, we construct a global matrix system by applying the Trefftz-FLAME molecule equations in each molecule. The global matrix system has the form  $[A]\{x\} = \{b\}$  and it can be solved using an iterative solver such as Conjugate Gradient. Here,  $[A]$  is a sparse banded matrix as in the standard finite difference method,  $\{x\}$  is a column vector of unknowns at each mesh node and  $\{b\}$  is defined by the excitation and boundary condition. As a solution of this linear system, we get the distribution of the field that can be used for further post-processing calculation such as the calculation of transmission and reflection coefficients for a waveguide.

## 1.3 Merits and drawbacks of Trefftz - FLAME

The main strength of Trefftz-FLAME comes from the fact that it incorporates local basis functions which can employ features of field distributions known a priori such as the field behavior in the vicinity of cylindrical and spherical particles. This procedure minimizes the “staircase” effects that can plague FDM at curved boundaries. In conventional FDM, modeling the boundary between two dissimilar materials presents difficulties. When a sampling node lies on the boundary between different materials one must decide what value to use for the constituent parameters. Obviously, this difficulty is

a source of error for electromagnetic problems that can be alleviated using the Trefftz-FLAME method.

Unlike FDM, it can be applied to curved surfaces with a far coarser mesh and provide results with the same accuracy as those provide by FEM when a very fine and geometrically conforming mesh is adopted [41]. Consequently, Trefftz-FLAME allows a huge reduction in the number of degrees of freedoms, especially in three dimensional problems. Moreover, it produces sparse, banded matrices that can be solved efficiently with iterative solvers. Unlike the previous Trefftz formulations based on FEM and BEM, this new method is neither a variational nor a Galerkin method. In addition, Trefftz-FLAME does not require a mesh generation step—only a simple Cartesian grid is required as in standard FDM.

A difficulty of Trefftz-FLAME is the determination of suitable local basis functions. For certain simple shapes (e.g. cylinders, spheres), these are available in closed form. Otherwise, they have to be computed numerically [36]. Trefftz-FLAME is particularly promising, then, for applications involving a large number of instances of the same structure, because the basis functions only have to be found once. An example is a Photonic Crystal device, made of many identical dielectric rods.

#### **1.4 Motivation, goals and thesis contribution**

The lack of efficient numerical techniques for solving problems that contain a large number of repeated structures is the main motivation for taking the Trefftz-FLAME technique and making further improvements. The research falls into two areas. The first concerns the two-dimensional Trefftz-FLAME for photonic crystal (PhC) structures. The goal is the accurate calculation of the reflection and transmission coefficients for devices built out of PhC waveguides. The second area is the development of a three dimensional, vectorial Trefftz-FLAME for the scattering of electromagnetic plane waves from multiple dielectric particles.

### 1.4.1 Photonic crystal devices

Photonic crystals [43, 44] are optical materials with periodic changes in the dielectric constant. Just as in semiconductors, band gaps can be created for certain ranges of frequency. We consider a square array of parallel, infinitely long, dielectric rods in air. The behavior of light in such a material can be understood by the analogy of an electron in solid-state crystals, because the dielectric particles can be regarded as “optical” atoms. The removal of rods breaks the periodicity in one spatial direction. This defect can introduce modes that decay exponentially away from the defect but can still be described by a wave vector pointing along the missing row or column of rods. Such a defect acts like a waveguide: waves of the right frequencies can propagate down the guide [43, 44]. Figure 1.1 shows a Y-branch device created by removing rods in a periodic structure. This and several other 2D photonic crystal devices will be analyzed in this thesis [45, 46].

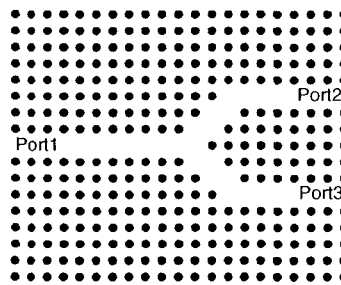


Figure 1.1 – Y-branch photonic crystal structure.

### 1.4.2 Aggregate of identical dielectric particles

This thesis will also address a problem of great interest to a broad range of scientific disciplines: the analysis of the electromagnetic scattering from an aggregate of dielectric particles [47-49]. For instance, Figure 1.2 depicts the scattering of a plane wave by a set of identical dielectric spheres. The radius is denoted by  $a$  and the relative permittivity is denoted by  $\epsilon_r$ . Analysis of a large but finite array of this sort can lead to a better understanding of optical band gaps in three dimensional structures. Despite mathematical complexities, a number of researchers have worked in the extended Mie theory [50, 51] to tackle this problem analytically. After a long history of development of

rigorous multiparticle scattering solutions, Xu et al. presented the Generalized Multiparticle Mie (GMM) method which is an extension of Mie based on the addition theorems for the vector spherical wave functions [52]. The GMM method provides an asymptotic representation of the total scattered far field from a set of randomly distributed dielectric spheres. Then, the expressions for the far field are used for deriving analytical expressions for pertinent scattering quantities, such as extinction and scattering cross section. It has been shown that his theoretical calculations agree favourably with experimental measurements for aggregates of 2, 3, 4, 8 and 27 identical spheres [53, 54]. These results will probably have an important role in benchmark tests to validate new numerical techniques for three dimensional scattering.

This theory provides expressions for the far fields, but there are instances where it is necessary to know the electromagnetic field within the particle. For instance, inelastically scattering radiation, such as florescent and Raman scattering by small particles, is stimulated by the internal field [55-58]. Also, the calculation of the internal electric field of a monolayer of periodically arrayed dielectric spheres provides fundamental knowledge on the origin of photonic bands that may be valuable in designing various kinds of PhC's [59].

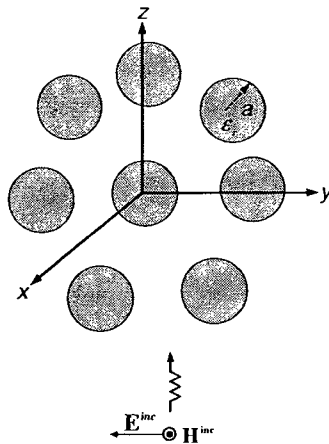


Figure 1.2 – A cluster of isotropic, homogeneous, and nonintersecting spheres of radius  $a$ , relative permittivity  $\epsilon_r$ , illuminated by a monochromatic plane wave.

The Vectorial 3D Trefftz-FLAME technique will provide an accurate calculation of the near field for the problem, including the field within the particles.

## 1.5 Outline of the thesis

A general formulation of Trefftz-FLAME is presented in Chapter 2. Then, in Chapter 3 2D Trefftz-FLAME is extended to incorporate the modal analysis and port boundary condition that are essential to an accurate calculation of reflection and transmission coefficients for a PhC devices. Comparisons with Finite Difference Time Domain (FDTD), multipole expansion and Finite Element Method (FEM) results are presented to show the efficiency and advantages of Trefftz-FLAME over these well established numerical techniques. Chapter 4 presents for the first time a new formulation: vectorial 3D Trefftz-FLAME for the scattering analysis of dielectric particles. It describes the local basis functions developed for the interior domain and for the absorbing boundary condition (ABC) as well. Then, numerical examples are presented for assemblies of dielectric spheres to show the accuracy, the convergence and, most importantly, the main merit of the developed technique: its ability to handle a spherical dielectric particle by using only a few molecules inside the sphere. Comparisons with the exact Mie solution and from well established numerical techniques are provided in order to verify the efficiency of the new technique. Finally, chapter 5 presents conclusions, lists original contributions, and discusses possible directions.

## Chapter 2

### The Trefftz-FLAME method

Here a general formulation of Trefftz-FLAME is presented. It is a Finite Difference-like approach that utilizes local basis functions that satisfy *a priori* the governing differential equation, instead of a Taylor series expansion as commonly used in the standard Finite Difference Method (FDM). Since the functions used are local, features known a priori such as the behavior of the field at curved boundaries can be incorporated directly into the numerical scheme.

A more comprehensive description of Trefftz-FLAME can be found in [10]. The version below differs slightly from the method described in [10], and avoids generalizations (e.g., to nonlinear operators) that are not relevant to the classes of problems tackled in this thesis.

#### 2.1 Basic formulation

First, we assume that a boundary-value problem can be defined by a governing differential equation in the domain  $\Omega$ :

$$L\mathbf{u} = 0 \quad (2.1)$$

together with the boundary conditions on the boundary  $\Gamma$  that encloses the domain. In Eq.(2.1),  $L$  is a differential operator and  $\mathbf{u}$  is the unknown quantity, which is assumed to be a vector field for generality.

First the computation domain  $\Omega$  is covered with a set of overlapping subdomains  $\Omega = \cup \Omega^{(p)}$ ,  $p = 1, \dots, n_g$ . Each subdomain contains a set of nodes  $i=0, \dots, n$ , which constitute a *stencil*, or *computational molecule*. For instance,  $n = 4$  defines a five-node stencil normally used in a standard Finite Difference approach, as shown in Figure 2.1

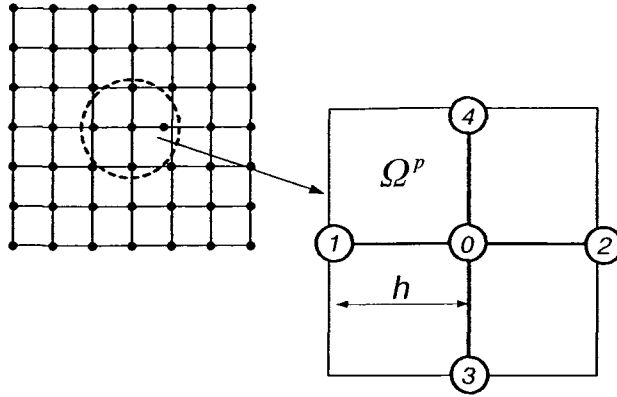


Figure 2.1 – A regular Finite Difference grid with a mesh size  $h$  and 5-node computational molecules.

Within each molecule there is a local approximation space  $\Psi^{(p)} = \text{span}\{\psi_k\}$ ,  $k = 1, 2, \dots, m$ , such that  $L\psi_k = 0$ . We represent  $\mathbf{u}$  locally by a linear combination of the basis functions  $\{\psi_k\}$ :

$$\mathbf{u}(\mathbf{r}) = \{\psi(\mathbf{r})\}^T \{c\} \quad (2.2)$$

where  $\mathbf{r}$  is the position vector.  $\{\psi\}$  is an  $m \times 1$  matrix whose vector entries are  $\psi_k$ .  $\{c\}$  is an  $m \times 1$  matrix containing the scalar coefficients  $c_k$ , to be determined later. We consider that a problem can be decomposed into a set of regions where different solutions can be assumed. For instance, if (2.1) is the wave equation and all the stencil nodes are in the same uniform region,  $\psi_k$  might be chosen to be plane waves. On the other hand, if the stencil contains part of a circular rod, as shown in Fig. (2.2), the functions  $\psi_k$  might be chosen to be cylindrical harmonics respecting the interface at the surface of the cylinder as well as satisfying the differential equation both inside and outside the cylinder.

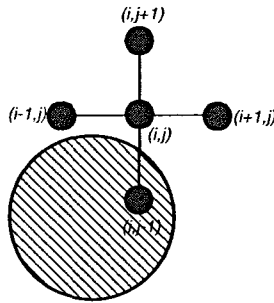


Figure 2.2 – Standard 5 node stencil crossing a curved interface.

Applying (2.2) at nodes  $i = 1, \dots, n$ , yields

$$\{\mathbf{u}\} = [\mathbf{M}]\{c\} \quad (2.3)$$

where  $\{\mathbf{u}\}$  is an  $n \times 1$  matrix with vector entries,  $\mathbf{u}_i = \mathbf{u}(\mathbf{r}_i)$ , and  $\mathbf{r}_i$  is the position vector of node  $i$ , and  $[\mathbf{M}]$  is a  $n \times m$  matrix with vector entries  $\mathbf{M}_{ik} = \psi_k(\mathbf{r}_i)$ , i.e.,

$$[\mathbf{M}] = \begin{bmatrix} \psi_1(\mathbf{r}_1) & \psi_2(\mathbf{r}_1) & \cdots & \psi_m(\mathbf{r}_1) \\ \psi_1(\mathbf{r}_2) & \psi_2(\mathbf{r}_2) & \cdots & \psi_m(\mathbf{r}_2) \\ \vdots & \vdots & \vdots & \vdots \\ \psi_1(\mathbf{r}_n) & \psi_2(\mathbf{r}_n) & \cdots & \psi_m(\mathbf{r}_n) \end{bmatrix} \quad (2.4)$$

To obtain the actual “difference” scheme for the molecule one needs to express the coefficients given by the vector  $\{c\}$  in (2.3) in terms of the vector of unknowns  $\{\mathbf{u}\}$ . We can modify the equation, so that,  $\{c\}$  can be isolated. Multiplying both sides of (2.3) by  $[\mathbf{M}]^T$ , the transpose of  $[\mathbf{M}]$ , yields

$$[\mathbf{M}]^T \cdot \{\mathbf{u}\} = [\mathbf{M}]^T \cdot [\mathbf{M}]\{c\} \quad (2.5)$$

Note that  $[\mathbf{M}]^T \cdot [\mathbf{M}]$  is a square,  $m \times m$ , scalar matrix, with the same rank as that of  $[\mathbf{M}]$ . Provided the rank of  $[\mathbf{M}]$  is  $m$ , therefore, the inverse  $([\mathbf{M}]^T \cdot [\mathbf{M}])^{-1}$  exists. Multiplying both sides of (2.5) by  $([\mathbf{M}]^T \cdot [\mathbf{M}])^{-1}$ , we get

$$\{c\} = ([\mathbf{M}]^T \cdot [\mathbf{M}])^{-1} ([\mathbf{M}]^T \cdot \{\mathbf{u}\}) \quad (2.6)$$

Equation (2.6) is the least-squares solution of (1.3). This means that  $\{c\}$  in (2.6) is not a solution to the system represented by (2.3) in the sense that it satisfies exactly every equation of the system. However  $\{c\}$  can be seen as the value such that  $\|[\mathbf{M}]\{c\} - \{\mathbf{u}\}\|$  is a minimum. As a result,  $\{c\}$  comes closest to satisfying all the equations. In other words,  $\{c\}$  is an appropriate “best solution”.

One can cast (2.6) in the following compact form:

$$\{c\} = [\mathbf{Q}] \cdot \{\mathbf{u}\} \quad (2.7)$$

where  $[\mathbf{Q}]$  is this  $m \times n$  matrix

$$[\mathbf{Q}] = ([\mathbf{M}]^T \cdot [\mathbf{M}])^{-1} [\mathbf{M}]^T \quad (2.8)$$

Next, we express the unknown field at the centre node of the computational molecule in terms of the unknowns at the surrounding nodes, in this way

$$\mathbf{u}_0 = \mathbf{u}_0(\mathbf{r}_0) = \{\boldsymbol{\psi}(\mathbf{r}_0)\}^T \{c\} \quad (2.9)$$

where,  $\mathbf{r}_0$  is the position vector of the centre node. Substituting (2.7) into (2.9) yields,

$$\mathbf{u}_0 = \{\boldsymbol{\psi}(\mathbf{r}_0)\}^T [\mathbf{Q}]\{\mathbf{u}\} \quad (2.10)$$

Equation (2.10) is a Trefftz-FLAME molecule equation, which is a discrete, local approximation to (2.1). By applying (2.10) to all the grid nodes, we get the global matrix system that has the following form

$$[A]\{x\} = \{b\} \quad (2.11)$$

here,  $[A]$  is a sparse matrix as in the standard finite difference method,  $\{x\}$  is a column vector of the unknowns at each mesh node and  $\{b\}$  is a vector arising from the excitation-boundary condition that will be discussed in later chapters. As a solution of this linear system, one gets a vector  $\{x\}$  that represents the field distribution. The system (2.11) can be solved using one of the several iterative solvers available, such as the Conjugate Gradient Method. More details about this formulation for particular problems, in two and three dimensions, will be presented in the next two chapters where it will be applied to the analysis of PhC devices and for the problem of wave scattering from dielectric spheres.

## Chapter 3

### Application of Trefftz-FLAME for Modeling Photonic devices

The scattering of electromagnetic radiation by a collection of objects with sizes comparable to the wavelength of incident radiation is a problem of considerable interest to a broad range of scientific applications. Among these is photonics. It has already been shown that FLAME is a very efficient numerical approach for solving problems containing many similar structures [34]. Indeed, Trefftz-FLAME has already been used to solve the wave equation inside a sharp  $90^\circ$  bend PhC waveguide [32]. However, to predict reflection and transmission properties two more steps are needed: first, to compute the dominant modes of the PhC waveguides attached to the ports [60]; second, to solve for the field in the device with the modes as the excitation, being careful to absorb the outgoing waves. This chapter presents an eigenvalue formulation of Trefftz-FLAME for finding the modes, and then it describes the formulation for an excitation-absorption boundary condition for use in predicting scattering in multi-port PhC devices. Finally, reflection and transmission coefficients of several devices are calculated by the new method; agreement with previously published values is excellent.

#### 3.1 Problem definition

We consider a two dimensional PhC device, where the computation domain is in the  $x$ - $y$  plane, as shown in Figure 3.1, and there is assumed to be no field variation in the  $z$  direction. Considering these assumptions and with a time-harmonic, transverse magnetic (TM) excitation, we obtain the following governing equation:

$$\nabla^2 \Phi + k^2 \Phi = 0 \quad \text{in } \Omega \quad (3.1)$$

where  $\Phi$  is the  $z$  component of the complex electric field;  $k = k_0 n_r$  is the wave number for the medium,  $k_0$  is the wave number for the free space,  $n$  is the refractive index of the medium and  $\Omega$  is the computational domain in the  $x$ - $y$  plane.

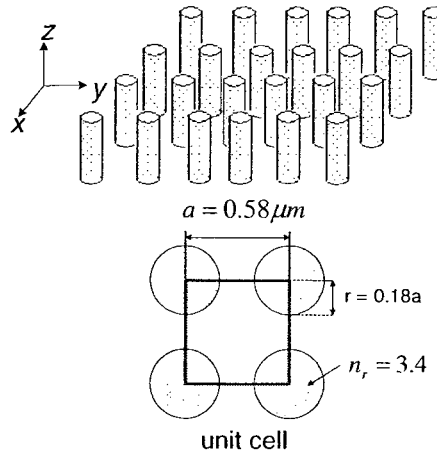


Figure 3.1 – Regular array of circular and infinitely long dielectric rods.

It is worth noticing that for an exactly periodic structure in  $x$  and  $y$ , as in Figure 3.1, the numerical analysis can be done considering only a unit cell and a periodic boundary condition. However, PhCs devices are not perfectly periodic. Their composition can be achieved from an initially perfect lattice shown in Figure 3.1, by removing rods, i.e., introducing “defects”. In this chapter the following devices will be modeled: a straight waveguide, a sharp  $90^\circ$  bend PhC, a Y-branch waveguide, a microcavity, a T-branch waveguide, and a directional coupler.

Consider an arbitrary  $N$ -Port optical structure representing a multiport PhC device, as depicted in Figure 3.2. At each port  $\Gamma_i$  is connected a PhC waveguide, which supports a propagating mode.  $V_i^+$  and  $V_i^-$  are two complex quantities defining the amounts of the incident and reflected waves at port  $i$ . To characterize the  $N$ -port device one must calculate the reflection,  $R_i$  and transmission,  $T_{ij}$ , power coefficients, respectively. To do this, first a computed mode is injected at the incident plane, indicated by  $\Gamma_i$ . Then, the electromagnetic field is evaluated for the whole domain using the FLAME method. Finally, using the computed field at each port one computes the power reflection  $R_i = |V_i^-/V_i^+|^2$  and transmission  $T_{ij} = |V_j^-/V_i^+|^2$  coefficients. The details of this method are given in the following sections.

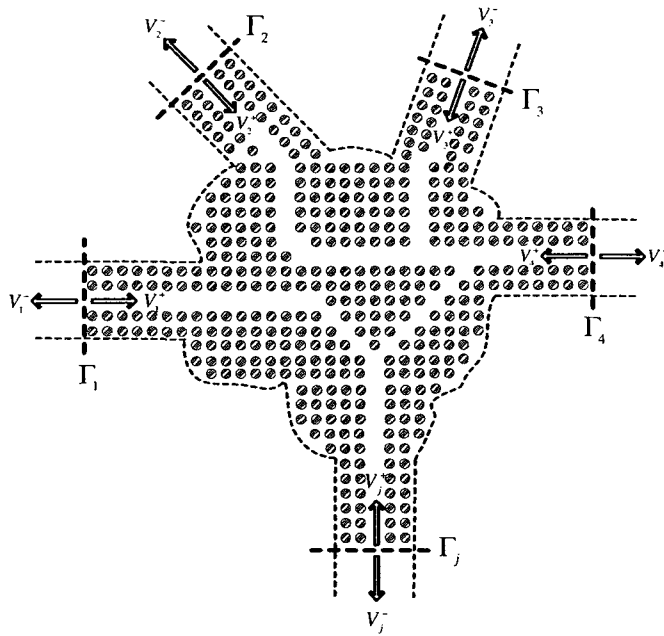


Figure 3.2 – A multiport optical device. One of ports is considered to be the input and the other ports are the output ports  $\Gamma_j$ .

### 3.2 Basis functions

Here, the basis functions are defined considering a nine-node stencil, as shown in Figure 3.3. It provides more accurate results in comparison with the standard five-node stencil [10], requiring only a modest increase in matrix bandwidth, and thus numerical effort.

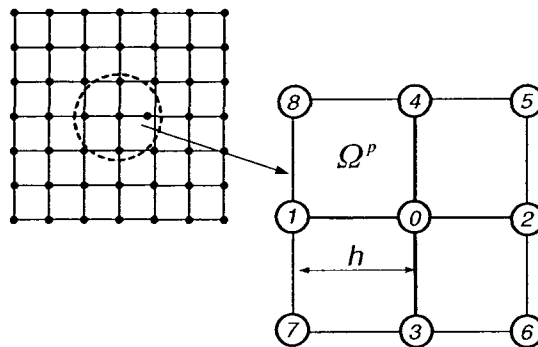


Figure 3.3 – A regular Finite Difference grid with a mesh size  $h$  and 9-node computational molecules.

As explained in Chapter 2, a key point of Trefftz-FLAME is the design of the basis functions. Here, two kinds of basis function are used: plane waves and cylindrical harmonics (solutions to the wave equation in cylindrical coordinates). Within stencils overlapping a rod, as indicated by Figure 3.4, we use cylindrical harmonics, otherwise, plane waves are chosen as basis functions.

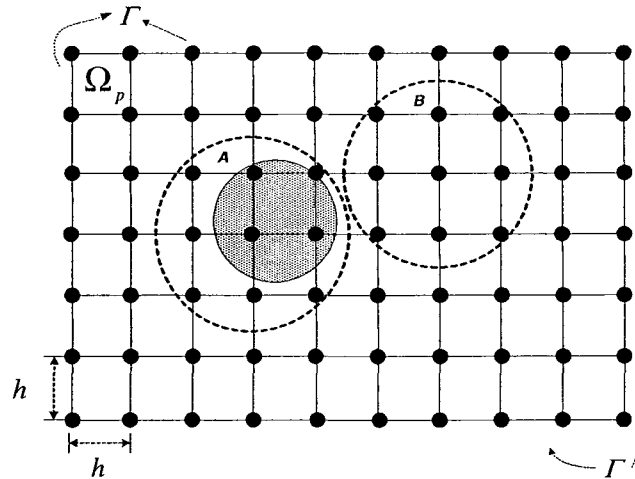


Figure 3.4 – Two dimensional grid with regular stencil of size  $h$ . Stencil A intercepts a rod and stencil B is in a uniform region.

### 3.3 Plane waves basis functions

The basis functions when no part of a rod is present in the molecule, are chosen to be 8 plane waves that propagate towards the central node in equally-spaced directions, as indicated in Figure 3.5.

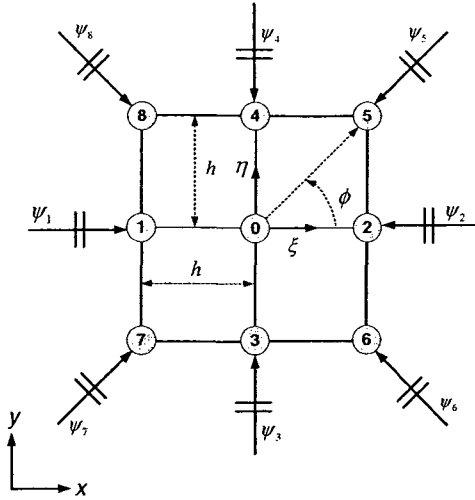


Figure 3.5 – Numbering of nodes for a nine-node stencil with 8 planes waves evenly distributed. A rectangular stencil with the same size  $h$  in both directions is used. The node 0 is in the origin of the stencil. Here  $\xi$  and  $\eta$  are local coordinates with an origin located at the centre of the molecule.

Within the molecule shown in Figure 3.5, a plane wave propagating in the  $\phi$  direction has a  $z$ -component of electric field of this form:

$$\psi = e^{-jk(\xi \cos \phi + \eta \sin \phi)} \quad (3.2)$$

here  $\xi$  and  $\eta$  are local coordinates, i.e., based on an origin that is the centre of the molecule as indicated in Figure 3.5

The eight basis functions, indicated by Figure 3.5, are:

$$\begin{aligned} \psi_1 &= e^{-jk\xi}, \quad \psi_2 = e^{jk\xi}, \quad \psi_3 = e^{-jk\eta}, \quad \psi_4 = e^{jk\eta}, \\ \psi_5 &= e^{jk\frac{(\xi+\eta)}{\sqrt{2}}}, \quad \psi_6 = e^{jk\frac{(\xi-\eta)}{\sqrt{2}}}, \quad \psi_7 = e^{-jk\frac{(\xi+\eta)}{\sqrt{2}}}, \quad \psi_8 = e^{-jk\frac{(\xi-\eta)}{\sqrt{2}}}. \end{aligned}$$

Thus, within each stencil that neither contains part of a dielectric rod nor has nodes on the external boundary  $\Gamma$ , the numerical solution is sought as a linear combination of these 8 plane waves.

### 3.4 Approximate absorbing boundary conditions (ABC)

Approximate absorbing boundary conditions have to be imposed at the outer boundary of the computational domain in order to suppress wave reflections back into the domain. The ABC is designed by using sets of plane waves with propagation directions that are out of the domain and along the side as shown in Figure 3.6.

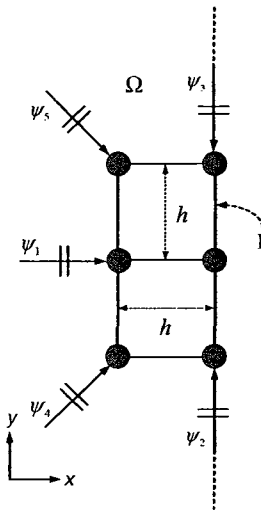


Figure 3.6 – Numbering of nodes for a six-node stencil that defines approximate absorbing boundary conditions (ABC) for the sides of the outer domain  $\Gamma$ . The stencil contains 5 plane waves evenly distributed. A rectangular stencil is used.

Also, there is an ABC for the corners of the domain. The basis consists of 3 plane waves propagating out of the domain, as shown in Figure 3.7.

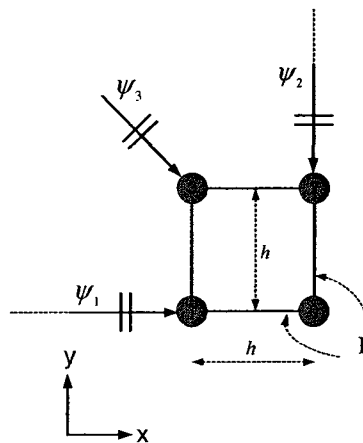


Figure 3.7 – Numbering of nodes for a three-node stencil that defines approximate absorbing boundary conditions (ABC) for the corners of the outer domain  $\Gamma$ . The stencil contains 3 plane waves evenly distributed. A square stencil is used.

### 3.5 Cylindrical harmonic basis functions

In order to model a dielectric cylinder we consider a set of basis functions that are the cylindrical harmonics that satisfy the governing Equation (3.1).

Consider an infinitely long dielectric cylinder. Here, the cylinder of radius  $r$  has refractive index  $n_{cyl}$  and is embedded in a dielectric medium of refractive index  $n_{out}$ , as shown in Figure 3.8. Moreover, the media are homogeneous, isotropic and source free.

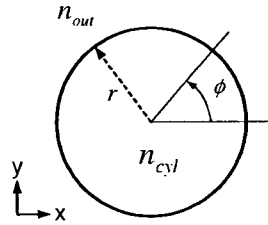


Figure 3.8 – Geometry of the cylinder.

The problem, above described, can be characterized by the following scalar wave equation in cylindrical polar coordinates  $\rho, \phi$  relative to the centre of the cylinder.

$$\frac{1}{\rho} \frac{\partial}{\partial \rho} \left( \rho \frac{\partial \Phi}{\partial \rho} \right) + \frac{1}{\rho^2} \frac{\partial^2 \Phi}{\partial \phi^2} + k^2 \Phi = 0 \quad (3.3)$$

where  $k = k_0 n_r$  is the wave number for the medium.

Following the method of separation of variables [52-54], we can express the solutions to (3), in terms of the following elementary wave functions:

$$\psi = t_n n_{cyl} k_0 \rho J_n(n_{cyl} k_0 \rho) e^{jn\phi} \quad \rho \leq r \quad (3.4)$$

$$\psi = [n_{out} k_0 \rho H_n^{(1)}(n_{out} k_0 \rho) + r_n n_{out} k_0 \rho H_n^{(2)}(n_{out} k_0 \rho)] e^{jn\phi} \quad \rho > r \quad (3.5)$$

with  $n = 0, \pm 1, \pm 2, \pm 3, \dots$

Here,  $t_n$  and  $r_n$  are the unknown coefficients, to be determined by the application of interface conditions at  $\rho = r$ . The function  $J_n(n_{cyl} k_0 \rho)$  is the Bessel function of the first kind, representing cylindrical standing waves;  $H_n^{(1)}$  is the Hankel function of first kind, representing inward-traveling waves;  $H_n^{(2)}$  is the Hankel function of the second kind, representing outward-traveling waves.

Matching the tangential components of the electric and magnetic fields, that are continuous at the interface ,  $\rho = r$  , we obtain:

$$r_n = \frac{\left(\frac{n_{cyl}}{n_{out}}\right) H_n^{(1)}(k_{out} r) J_n'(k_{cyl} r) - J_n(k_{out} r) H_n'^{(1)}(k_{cyl} r)}{J_n(k_{cyl} r) H_n'^{(2)}(k_{out} r) - \left(\frac{n_{cyl}}{n_{out}}\right) H_n^{(2)}(k_{out} r) J_n'(k_{cyl} r)} \quad (3.6)$$

$$t_n = \frac{\left(H_n^{(1)}(k_{out} r) H_n'^{(2)}(k_{out} r) - J_n(x_{cyl}) H_n'^{(1)}(k_{cyl} r)\right)}{J_n(k_{cyl} r) H_n'^{(2)}(k_{cyl} r) - \left(\frac{n_{cyl}}{n_{out}}\right) H_n^{(2)}(k_{out} r) J_n'(k_{cyl} r)} \quad (3.7)$$

where  $' = \frac{\partial}{\partial(k\rho)}$ ,  $k_{out} = \left(\frac{2\pi}{\lambda}\right)n_{out}$ ,  $k_{cyl} = \left(\frac{2\pi}{\lambda}\right)n_{cyl}$  and  $\lambda$  is the wavelength for free space.

With these values of  $r_n$  and  $t_n$ , (3.4) and (3.5) define basis function that satisfies the wave equation and the interface conditions across the rod boundary. We need 8 basis functions of this kind for the standard 9-node stencil, and they are constructed by choosing  $n = -3, -2, -1, 0, 1, 2, 3, 4$ .

It is important to note that this computational molecule can not overlap more than one rod since the expressions for the basis functions are derived for a single rod.

### 3.6 Applying the Trefftz-FLAME method

In the Trefftz-FLAME method, the starting point is a regular two dimensional grid of nodes over  $\Omega$  as shown Figure 3.4.

As defined in Chapter 2, the Trefftz-FLAME molecule equation, which is a discrete, local approximation to (1.1), is given by

$$\mathbf{u}_0 = \{\psi(\mathbf{r}_0)\}^T [\mathbf{Q}]\{\mathbf{u}\} \quad (3.8)$$

where  $[\mathbf{Q}]$  is an  $m \times n$  matrix

$$[\mathbf{Q}] = ([\mathbf{M}]^T \cdot [\mathbf{M}])^{-1} [\mathbf{M}]^T \quad (3.9)$$

In this two dimensional formulation the unknown is a scalar (a single component of the electric field). Therefore the sets of basis functions are scalar quantities. Then (3.9) is reduced to

$$[Q] = ([M]^T [M])^{-1} [M]^T \quad (3.10)$$

$$[M] = \begin{bmatrix} \psi_1(\mathbf{r}_1) & \psi_2(\mathbf{r}_1) & \cdots & \psi_m(\mathbf{r}_1) \\ \psi_1(\mathbf{r}_2) & \psi_2(\mathbf{r}_2) & \cdots & \psi_m(\mathbf{r}_2) \\ \vdots & \vdots & \vdots & \vdots \\ \psi_1(\mathbf{r}_n) & \psi_2(\mathbf{r}_n) & \cdots & \psi_m(\mathbf{r}_n) \end{bmatrix} \quad (3.11)$$

i.e., both  $[M]$  and  $[Q]$  are scalar matrices. Moreover, for each of the molecules discussed above the number of basis functions is equal to the number of nodes, that is  $m = n$ . Then  $([M]^T [M])^{-1} = [M]^{-1} [M]^T$  and  $[Q] = [M]^{-1}$ . So Equation (3.8) for the scalar, two dimensional problem is reduced to the form

$$\mathbf{u}_0 = \{\psi(\mathbf{r}_0)\}^T [M]^{-1} \{\mathbf{u}\} \quad (3.12)$$

By applying (3.12) to all the grid nodes, we get the following global matrix system, as described in Chapter 2

$$[A]\{x\} = \{b\} \quad (3.13)$$

where,  $\{x\}$  are the values of the  $x$ -component of the electric field at the mesh nodes and  $\{b\}$  is a vector arising from the excitation-boundary condition that will be discussed later in this chapter.

### 3.7 Trefftz-FLAME for the waveguide mode calculation

In general, the waveguide connected to a port can support multiple modes of propagation for a specific excitation frequency. However, the PhC devices analyzed in this chapter allow only the dominant mode to propagate. In order to apply a suitable boundary condition to the ports, it is first necessary to compute the field of the dominant mode of the waveguide passing through that port, together with its phase constant,  $\beta$ . Figure 3.9 shows a port with a short length of waveguide connected to it, and a FLAME grid superimposed. As shown in Figure 3.9 a waveguide in a PhC is periodic in the

propagation direction, but the symmetry in the other direction is broken by the line of defects or vacancy of rods. When we assume that  $x$  is the waveguide direction and  $a$  accounts for the periodicity in this direction, the Floquet theorem can be applied to a unit cell, the shaded region in Figure 3.9. The governing equation remains (3.1), with the value of  $\omega$  as required for the subsequent scattering analysis. On lines  $\Gamma_1$  and  $\Gamma_2$  it is necessary to apply the Floquet boundary condition  $\phi(a, y) = \mu\phi(0, y)$ , where  $\mu = e^{-i\beta a}$ . This is done as follows. An extra row of nodes placed outside the port, as shown in Figure 3.9. For nodes  $i=1, \dots, M-1, j=1, \dots, N$ , the same Trefftz-FLAME equations are constructed as described in the previous section – including the use of ABC-FLAME for the nodes on the left and right boundaries ( $j=1$  and  $j=N$ ).

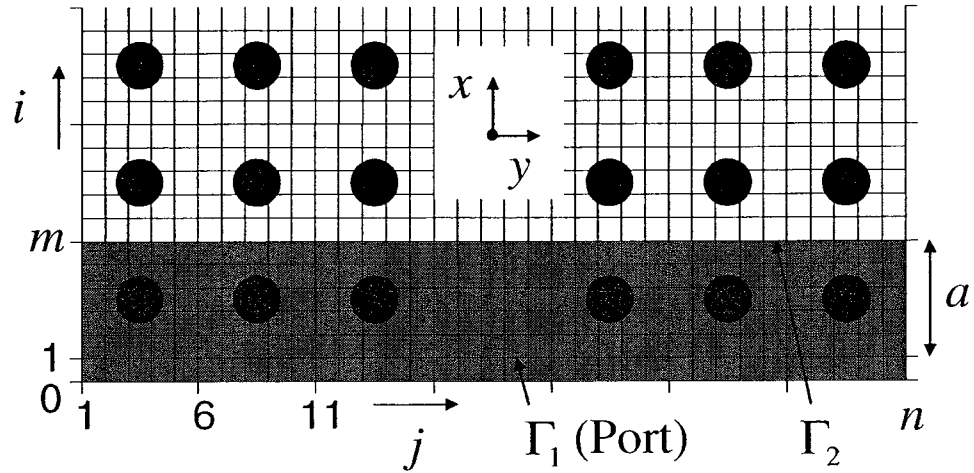


Figure 3.9 – A port and a short length of a typical PC waveguide. The waveguide axis is in the  $x$  direction. Energy is largely confined to the “defect” in the middle. The shaded area is used for finding the modes.

Then the following  $2N$  equations are added, to enforce the periodic condition:

$$\begin{aligned}\phi_{Mj} &= \mu\phi_{1j} \quad j=1, \dots, N \\ \phi_{M-1,j} &= \mu\phi_{0j} \quad j=1, \dots, N\end{aligned}\tag{3.14}$$

The result is  $(M+1)N$  equations in the same number of nodal unknowns. The parameter  $\mu$  is also unknown, but becomes the eigenvalue. The set of equations can be arranged into this form:

$$[A]\{\phi\} = \mu[B]\{\phi\}\tag{3.15}$$

Matrices  $[A]$  and  $[B]$  are sparse, but not Hermitian; since they are relatively small, the MATLAB dense-matrix QZ algorithm can be used for the eigenproblem. This gives  $\phi^+$ , the dominant mode propagating in the  $+x$  direction along the periodic waveguide, along with its associated value of  $\mu$ , from which  $\beta$  is obtained. It also gives  $\phi^-$ , the dominant mode propagating in the  $-x$  direction. By symmetry,  $\phi^-$  has phase constant  $-\beta$ , and provided  $\phi^+$  and  $\phi^-$  are normalized in the same way we have:

$$\begin{aligned}\phi_{1j}^- &= \phi_{Mj}^+ & j=1, \dots, N \\ \phi_{Mj}^- &= \phi_{1j}^+ & j=1, \dots, N\end{aligned}\tag{3.16}$$

### 3.8 The Port Boundary Condition

As already mentioned, the computed mode is then incorporated into an excitation-absorption boundary condition for use in predicting scattering in multi-port PhC devices. Let  $\phi^+$  and  $\phi^-$  correspond to waves incident on a port and leaving a port, respectively. Then if we assume that only these fields are present, the total field on the port is given by:

$$\phi = V^+ \phi^+ + V^- \phi^- \tag{3.17}$$

where  $V^+$  and  $V^-$  are two complex coefficients defining the amounts of the incident and outgoing waves, respectively. We specify  $V^+$  for each port, but do not know  $V^-$ ; we need a boundary condition that sets up the incident wave and absorbs the outgoing wave. From (3.14) and (3.17):

$$\begin{aligned}\phi_{1j} &= V^+ \phi_{1j}^+ + V^- \phi_{1j}^- & j=1, \dots, N \\ \phi_{Mj} &= V^+ \phi_{Mj}^+ + V^- \phi_{Mj}^- = V^+ \phi_{1j}^+ e^{-j\beta a} + V^- \phi_{1j}^- e^{j\beta a} & j=1, \dots, N\end{aligned}\tag{3.18}$$

Eliminating  $V^- \phi_{1j}^-$  from these equations gives:

$$e^{j\beta a} \phi_{1j} - \phi_{Mj} = V^+ \phi_{1j}^+ 2j \sin \beta a \quad j=1, \dots, N \tag{3.19}$$

This set of equations replaces the usual Trefftz-FLAME equations (3.12) for nodes along the port  $i=1$ , and constitutes the boundary condition needed for the port. Note that, for an unexcited port,  $V^+$  is set to zero. It is also worth pointing out that the terminal plane or input port has to be far enough from the junction to allow the decay of evanescent modes.

### 3.9 Scattering Analysis

The whole structure is modeled by the global Equation (3.13) assembled using Trefftz-FLAME method as previously mentioned. Here,  $\{b\}$  is defined by imposing the right hand side of the port-boundary condition given by (3.19).

After solving the global system, the value of  $V^-$  can be extracted using equations (3.17)- (3.19):

$$\begin{aligned}\phi_{1j} &= V^+ \phi_{1j}^+ + V^- \phi_{1j}^- \\ &= V^+ \phi_{1j}^+ + V^- \phi_{mj}^+ = V^+ \phi_{1j}^+ + V^- \phi_{1j}^+ e^{-j\beta a} \quad j=1, \dots, N\end{aligned}\quad (3.20)$$

Rearranging:

$$V^- = (\phi_{1j} - V^+ \phi_{1j}^+) / (\phi_{1j}^+ e^{-j\beta a}) \quad j=1, \dots, N \quad (3.21)$$

In theory, each node  $j$  should give the same value of  $V^-$ ; in practice, the right hand side of (3.21) is averaged over all the nodes on the port.

The power reflection coefficients given in the next section are the values  $|V^-/V^+|^2$ .

The same expression is used for the transmission coefficients, but in this case  $V^+$  is for one port and  $V^-$  for another (with the same waveguide dimensions at each). The coefficients are plotted directly as ratios, rather than in dB, since this is customary in the PhC literature.

### 3.10 Numerical results

In order to validate the method, the reflection and transmission coefficients of several devices are calculated: a sharp 90° waveguide bend, a Y-branch waveguide, a directional coupler, a T-branch waveguide and a microcavity. All results are compared with published results computed by means of well established formulations such as the Beam Propagation Method and FDTD.

For all simulations the waveguides are made of a square lattice of dielectric rods (refractive index 3.4) in air. Each rod is circular with radius  $r = 0.18 a$ , where  $a$  is the lattice constant.

In order to treat PhC waveguides, first, the eigenmodes of the periodic waveguide are calculated following the method described in the previous section. Figure 3.10 shows the normalized propagation constant  $\beta a / 2\pi$  of the TM mode guided along a line defect, as a function of normalized frequency  $\omega a / (2\pi c)$ . The results show that we can model the  $a \times a$  lattice cell with  $6 \times 6$  points and obtain results that agree well with those of the plane wave expansion (PWE) method [64].

Next, we apply FLAME to a  $90^\circ$  bend. The fundamental TM mode is incident at port 1. Figure 3.11 shows that the results obtained using  $8 \times 8$  nodes per lattice cell, giving 7,744 degrees of freedom (DOF). These results agree well with those calculated by the FE Time-Domain Beam Propagation Method (FETD-BPM) using 158,607 DOFs [64]. Note that at one frequency the FLAME transmission coefficient is very slightly greater than 1 (actually 1.016). This is the result of discretization error; nothing in FLAME, explicitly imposes power conservation.

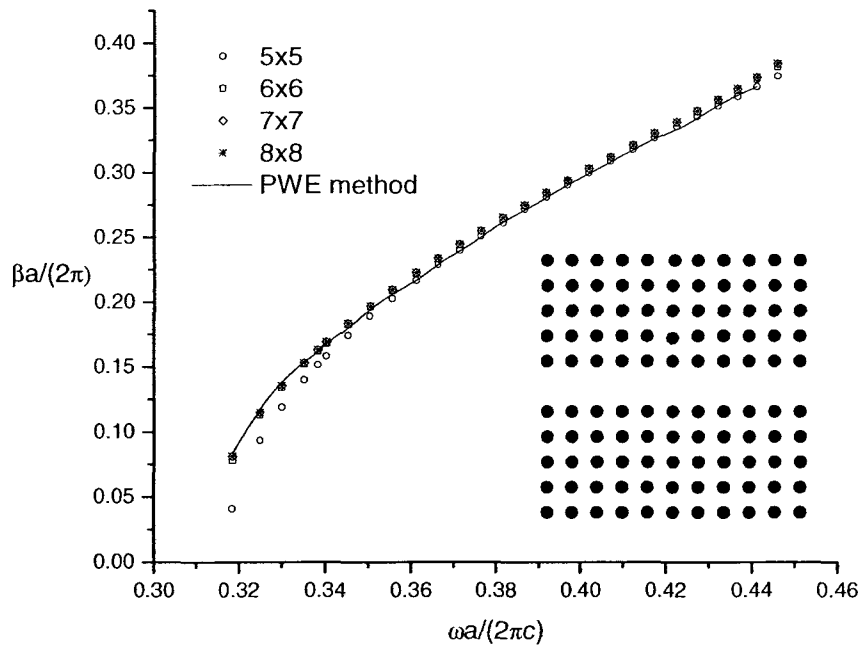


Figure 3.10 – Dispersion curves for a PC waveguide. The  $a \times a$  lattice cell is modeled with  $5 \times 5$  (circles),  $6 \times 6$  (squares),  $7 \times 7$  (triangles) and  $8 \times 8$  (stars) grid points. The solid line is from [64], obtained by the PWE method.

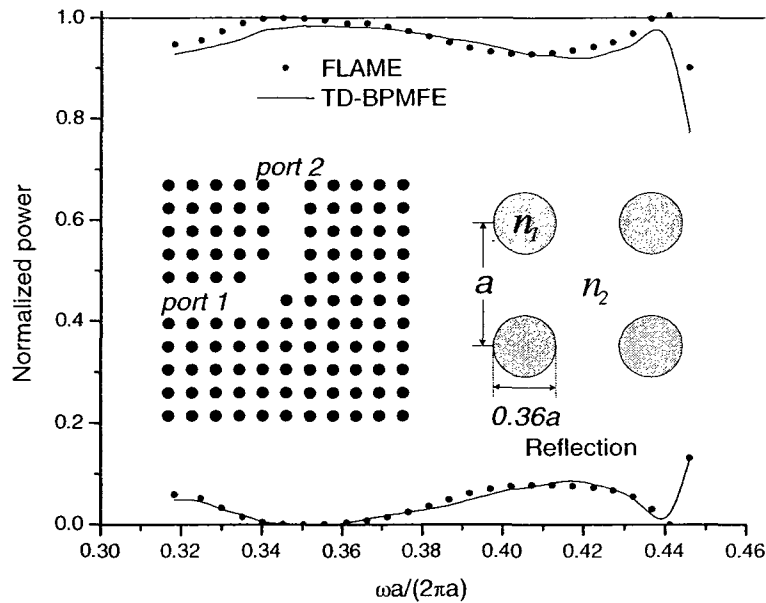


Figure 3.11 – Transmission and reflection coefficients of a sharp 90° waveguide bend. Circles represent FLAME and solid lines represent FETD-BPM [65] results.

Figure 3.12 shows, for the same device, the transmission and reflection coefficients as a function of normalized frequency  $\omega a/(2\pi c)$  when the lattice cell is modeled with 5×5, 6×6, 7×7 and 8×8 nodes. It can be seen that the convergence is fast and that there is no significant difference in the results when 6×6, 7×7 or 8×8 grid points are used.

The FLAME results for a Y-branch are shown in Figure 3.13. Port 1 is excited and from the field solution the reflection coefficient at port 1 and the transmission coefficients to ports 2 and 3 were computed. The results obtained are in very good agreement with those of FETD-BPM [65].

Next, we apply FLAME to a T-branch, Figure 3.14. Again, port 1 is excited. FLAME results agree well with those of the Finite Difference Time Domain (FDTD) method [66], also plotted. In the FDTD simulation the lattice cell was modeled with 15×15 grid points, whereas in the FLAME simulation only 8×8 grid points were used.

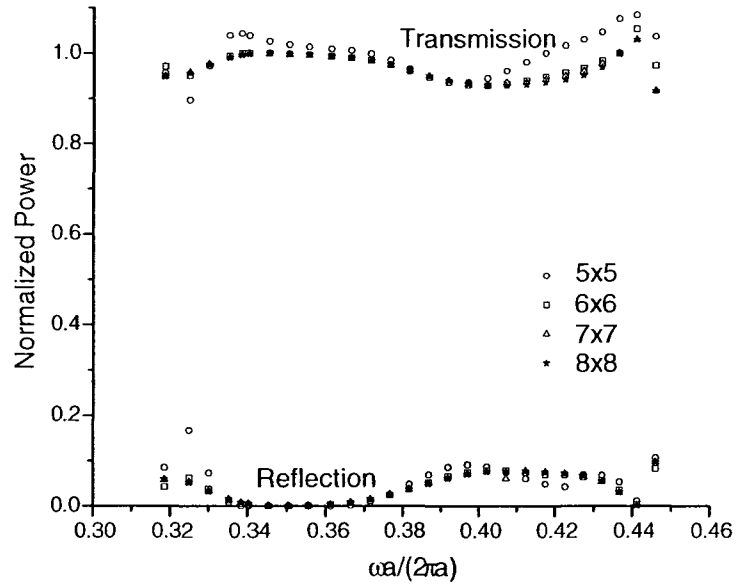


Figure 3.12 – Convergence of the results for the PhC bend (Figure 3.11). The lattice cell is modeled with 5×5 (circles), 6×6 (squares), 7×7 (triangles) and 8×8 (stars) grid points.

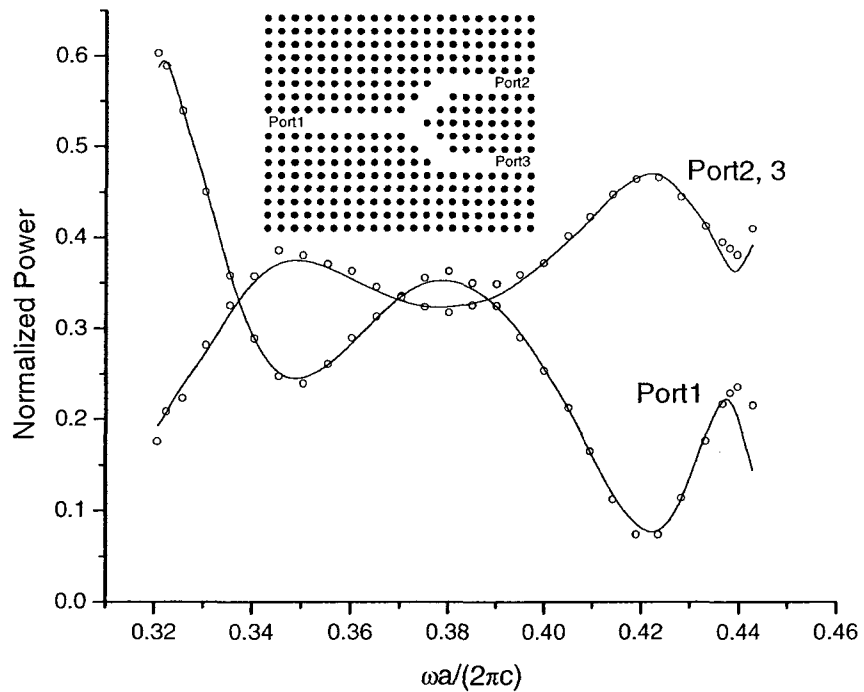


Figure 3.13 – Transmission and reflection coefficients of a Y - branch waveguide. Circles represent FLAME and solid lines represent FETD-BPM [65] results.

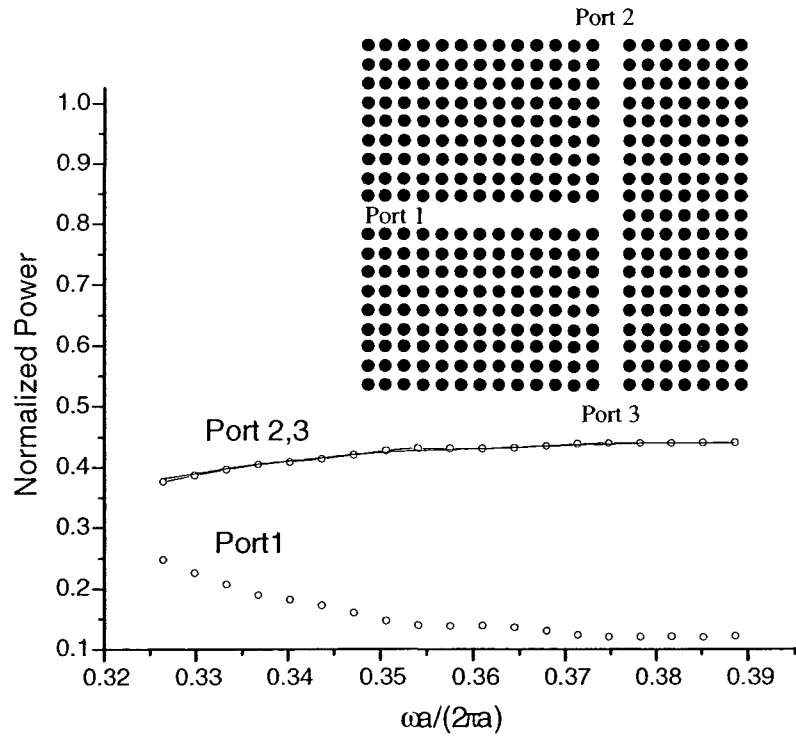


Figure 3.14 – Transmission and reflection coefficients of a T-branch waveguide. Circles represent FLAME and the solid line represents FDTD results [66].

An example of a 4-port device is the directional coupler shown in Figure 3.15. Power injected at port 1 is coupled to the three other ports to varying degrees. Once again, there is good agreement with FETD-BPM results [66].

Finally, we consider a microcavity coupled to straight waveguides (Figure 3.16). At the frequency of cavity resonance, there is a strong transmission from port 1 to port 2, which FLAME is able to capture.

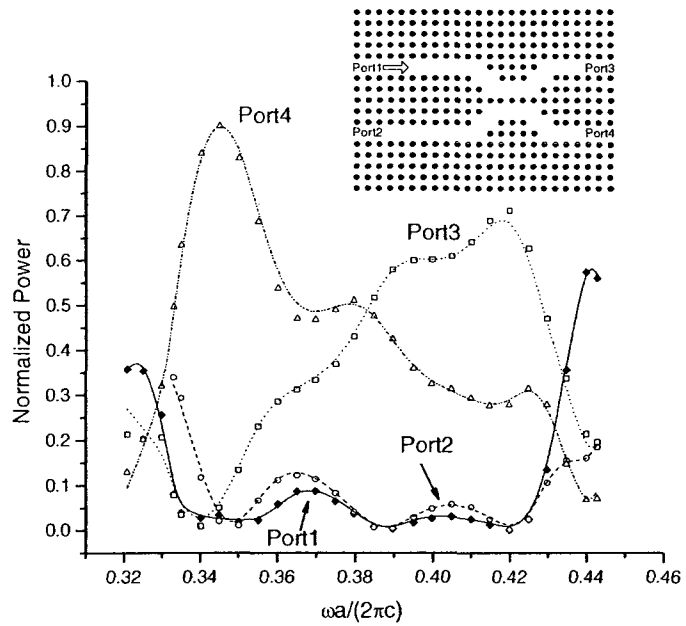


Figure 3.15 – Transmission and reflection coefficients of a directional coupler. Circles, squares, triangles and solid diamonds represent FLAME results and the lines represent FETD-BPM results [66].

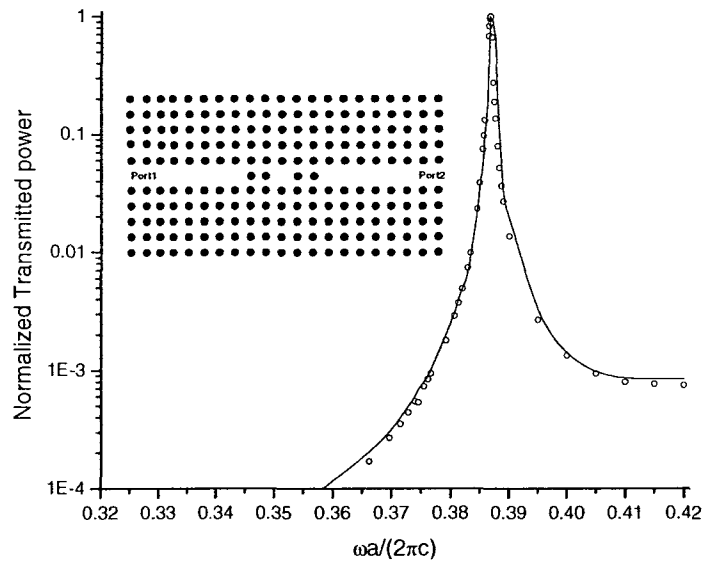


Figure 3.16 – Transmission coefficient of a microcavity. Circles represent FLAME results and the solid line represents FETD-BPM results [66].

TABLE 3.1  
RELATIVE EFFICIENCY OF FLAME

	METHOD	REF.	RODS	DOFs
STRUCTURE				
Bend	FLAME		11 x 11	7,744
	FETD-BPM	[37]	638	158,607
	FDTD	[38]	101 x 121	
Y-Branch	FLAME		21 x 17	22,848
	FETD-BPM	[37]	65 x 17	
Coupler	FLAME		24 x 17	26,112
	FETD-BPM		65 x 17	
T-Branch	FLAME		21 x 19	25,536
	FDTD	[39]	141 x 181	5,742,225
Microcavity	FLAME		19 x 11	13,376
	FETD-BPM		65 x 11	

Some idea of the relative efficiency of the FLAME approach to PhC device analysis is given by Table 3.1, which gives the number of rods in the computational domain and the number of degrees of freedom, for FLAME and for competing methods. In each case, the computational domain (number of rods) needed by FLAME is significantly smaller than for FETD-BPM and FDTD. This, together with the coarser gridding needed per lattice cell, gives a much lower number of degrees of freedom. The FLAME matrices are not only modest in size, they are also very sparse. Solution times

for the matrix problem using a direct, sparse solver were less than 2 seconds per frequency point (on a Pentium 4, 3 GHz processor), for all of the problems presented.

### 3.11 Discussions

A two dimensional Trefftz-FLAME has been presented for computing the propagating mode of a PhC waveguide. It has been shown how the computed mode can be used to provide port boundary conditions for a PhC multiport device, and to extract reflection and scattering coefficients. Reflection and transmission coefficients of several devices have been calculated by the new method; agreement with previously published values is excellent. This computational efficiency is the result of FLAME's ability to model the circular rods with a relatively coarse grid, and is also due to the small size of the computational domain needed for this frequency-domain, mode-driven analysis. Although only square lattices have been tried so far, the method could equally be applied to other lattice types, e.g., triangular. Furthermore, it could also be used for the analysis of PhC devices based on air pores (hollows) in a solid medium.

In the next chapter, the Trefftz-FLAME is extended to 3D geometries, more specifically, to an aggregate of dielectric spheres.

## Chapter 4

### **Vectorial 3D FLAME for the scattering analysis of dielectric particles**

The study of light scattering by an aggregate of small particles is a fundamental problem in the electromagnetic theory. It has a tremendous importance in various disciplines from physics, sensors, photonics, chemistry, environmental sciences to biology, process diagnostics and medicine [48, 49]. For instance, arrays of dielectric spheres are valuable in understanding the physics of 3D photonic crystals [67]. Indeed, the Mie theory has already been extended to the classical problem of electromagnetic scattering by aggregates of arbitrarily configured non identical isotropic and homogeneous spheres [50-54].

Numerical solutions are indispensable because they can offer solutions for nonspherical geometries and complex media. Nevertheless, due to the computational overhead, only a small number of techniques have been reported that focus on numerical treatment of three-dimensional structures composed of a number of repeated scatterers. For example, in [9] a Domain Decomposition technique combined with FEM has been applied to 3D photonic crystals. The Trefftz-FLAME method is an alternative technique for studying a system of many particles, whether the particles are assumed to be displaced from a random distribution, e.g., carbon dust particles and living cells [49], or a uniformly ordered distribution, as in photonic crystals.

As described in the previous chapters, Trefftz-FLAME has been proven to be a very effective computational technique for solving problems involving large numbers of similar structures [32, 34]. In the present chapter, Trefftz-FLAME is developed for the

three-component phasor electric field in and around scatterers when a plane wave is incident. To date, its application in 3D has been limited to scalar problems with Dirichlet boundary conditions [34]. The extension to 3D is conceptually immediate, but the effort in the formulation development is greatly increased due to the challenging task of finding local basis functions that can capture not only the vectorial nature of the problem but also circumvent ill-conditioning problems that can hamper the use of this technique in any practical problem. As a matter of fact, the main effort in developing a 3D Vectorial Trefftz-FLAME formulation is to define basis functions without incurring additional computational problems due to a high condition number for the matrices.

#### 4.1 Statement of the problem

We consider an arbitrarily configured cluster of  $L$  particles, as shown in Figure 4.1, with complex relative permittivity,  $\epsilon_r^j$ , and complex relative permeability,  $\mu_r^j$ ,  $j = 1 \dots L$ . Throughout this chapter, any single integer in a right-hand superscript, such as  $j$  in  $a^j$ , indicates that the quantity is related to the  $j^{\text{th}}$  particle. We also assume that the aggregate of particles are confined to a finite volume that is illuminated by a  $z$ -propagating monochromatic plane wave as indicated in Figure 4.1.

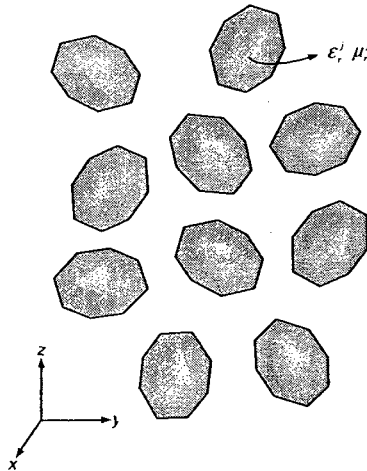


Figure 4.1 – Scatterers of repeated shape, randomly distributed. Here,  $x, y, z$  represents a *global* Cartesian coordinate system.

The time-harmonic electric field  $\mathbf{E}$  for the problem above satisfies the vector wave equations in a source-free region

$$\nabla \times \left( \frac{\nabla \times \mathbf{E}}{\mu_r} \right) - k_0^2 \epsilon_r \mathbf{E} = 0, \quad (4.1)$$

where  $k_0$  is the wave number for free space,  $\epsilon_r$  is the relative permittivity; and  $\mu_r$  is the relative permeability of the medium.

Trefftz-FLAME computes the local field both inside and outside the particles. It is worth pointing out that there has been an increasing interest in near-field calculation due to the rapid development of areas such as single-molecule spectroscopy by surface-enhanced Raman scattering (SERS), nanodevices based on surface plasmon photonic forces, high spatial resolution of near-field optical microscopy and quantum-optical processes in photonic crystals [55-59].

## 4.2 Applying the Trefftz - FLAME method

The method is essentially as described in chapter 2, but with one difference: since the problem involves the scattering of an incident plane wave, the electric field of the plane wave,  $\mathbf{u}^{inc}$ , is added explicitly to the approximation:

$$\mathbf{u}(\mathbf{r}) = \sum_{k=1}^m c_k \boldsymbol{\psi}_k + \mathbf{u}^{inc}(\mathbf{r}) \quad (4.2)$$

Carrying out the procedure presented in chapter 2, we obtain the following 3 equations for a computational molecule

$$\mathbf{u}_0 - \{\boldsymbol{\psi}(\mathbf{r}_0)\}^T [\mathbf{Q}]\{\mathbf{u}\} = \mathbf{u}^{inc}(\mathbf{r}_0) - \{\boldsymbol{\psi}(\mathbf{r}_0)\}^T [\mathbf{Q}]\{\mathbf{u}^{inc}\} \quad (4.3)$$

The vectors  $\{\boldsymbol{\psi}\}$  and matrix  $[\mathbf{Q}]$  are defined in chapter 2.

### 4.2.1 Computational Molecule

The method uses a 19 node-stencil that has proven to be a highly accurate stencil for the conventional FD method that uses Taylor series [70,72]. The 19-node

computational molecule adopted is a cubic cell  $3 \times 3 \times 3$  with the 8 corner nodes removed as shown in Figure 4.2. Then, the labeling of the 3D molecule is given in Figure 4.3.

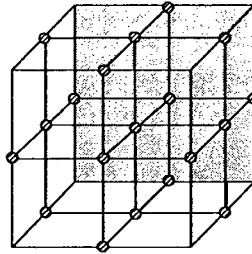


Figure 4.2 – The 19 node cubic cell. The circles represent a 19 - node computational molecule.

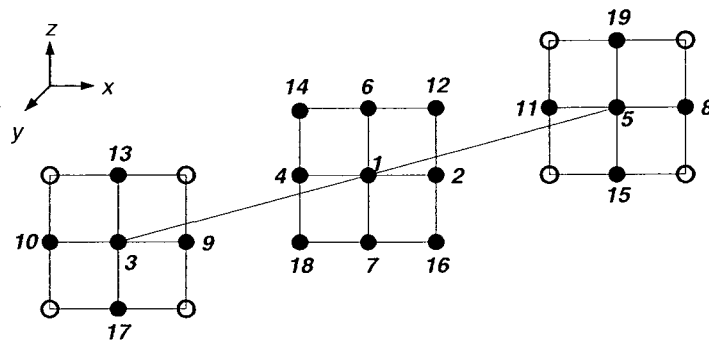


Figure 4.3 – Labeling of the 3D grid points in a 19-node computational molecule.

#### 4.2.2 Basis Functions

We consider a collection of scatterers randomly distributed and oriented in the global  $x, y, z$  coordinate frame. The position of each scatterer is defined by the coordinates  $x^j, y^j, z^j$  of the origin of its local coordinates ( $O^j$ ) as indicated in Figure 4.4.

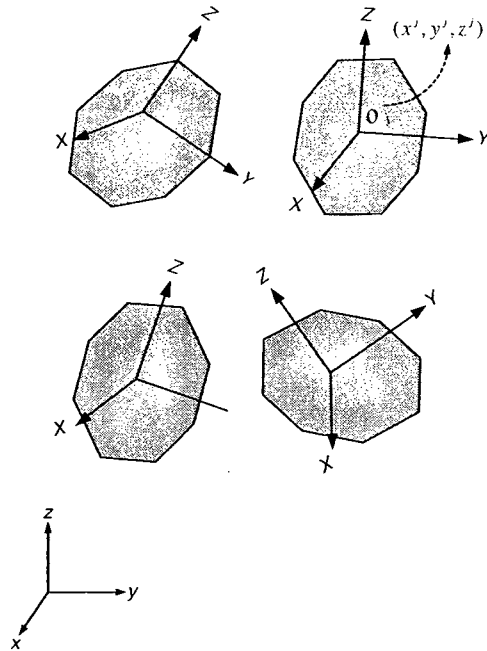


Figure 4.4 – A random distribution of scatterers. The coordinates  $x, y, z$  represent the global system and the axes  $X, Y, Z$  are the local system of the  $j^{\text{th}}$  scatterer.

Basically, the procedure for finding the basis functions is divided into three steps. In the first step we specify a set of incident plane waves  $\tilde{\psi}^{inc}$  in the local,  $X, Y, Z$  coordinate frame of the scatterer. In the second step, the total field resulting from the interaction of each incident wave with the scatterer is found, again in the local frame. Each such total field is a basis function,  $\tilde{\psi}$ . Finally, in the last step, the basis functions are mapped to the global coordinates  $x, y, z$ .

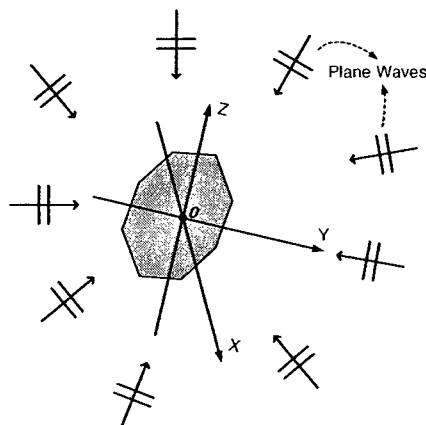


Figure 4.5 – Representation of a procedure to generate basis functions in the local frame  $X, Y, Z$ .

The distribution of incident waves represented in Figure 4.5 must be symmetric to ensure that basis functions are not favored in biased directions. Additionally, ill-conditioning of the final global matrix is avoided if the basis functions are as linearly independent as possible. Numerical experiments have shown that 36 plane waves, divided in two polarizations propagating in 18 directions symmetrically arranged around the centre node, give good results. Each direction is parallel to a line connecting one of the 18 nodes of the molecule to the centre node as represented in Figure 4.6.

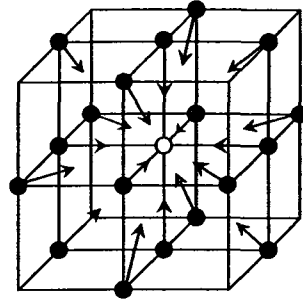


Figure 4.6 – The arrows define plane waves propagating in 18 directions symmetrically arranged around the centre node.

Each basis function is the solution obtained for a specific plane wave, and it is expressed as

$$\tilde{\Psi} = \tilde{\Psi}^{inc} + \tilde{\Psi}^{sca} \quad (4.4)$$

#### 4.2.2.1 STEP 1: the set of incident waves

The different plane waves can be generated by rotation of a canonical wave: a single incident wave propagating in the +Z direction as shown in Figure 4.7, polarized along the X axis:

$$\tilde{\Psi}_c^{inc}(\mathbf{R}) = \mathbf{a}_x e^{-jkZ} \quad (4.5)$$

where  $\mathbf{R} = \begin{Bmatrix} X \\ Y \\ Z \end{Bmatrix}$  is the position vector expressed in local coordinates.

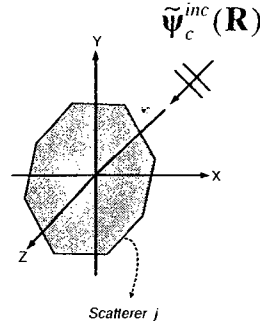


Figure 4.7 – A general single scatterer with incident wave propagating in the +Z direction.

Another incident plane wave, propagating in the +Z' direction, is created by using the same function in the rotated frame X', Y', Z' as depicted in Figure (4.8) :

$$\tilde{\Psi}_c^{inc}(\mathbf{R}') = \mathbf{a}'_x e^{-jkZ'} \quad (4.6)$$

where  $\mathbf{R}' = \begin{Bmatrix} X' \\ Y' \\ Z' \end{Bmatrix}$ . The rotation can be defined by two angles  $\theta_k$  and  $\varphi_k$  as shown in

Figures 4.8. First, a rotation  $\varphi_k$  is applied about Z. Then, a second rotation by  $\theta_k$  is applied about the Y' axis as demonstrated in Figure 4.8.

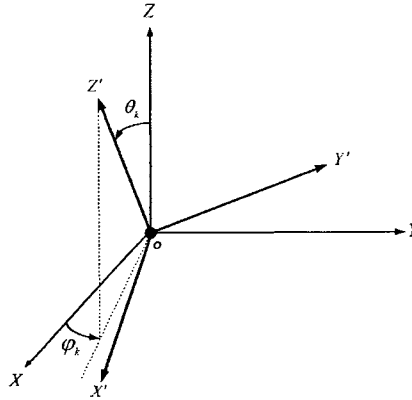


Figure 4.8 – A plane wave in the rotated frame X', Y', Z'.

The overall effect is expressed by the following rotation matrix [78]:

$$\mathbf{R}' = \mathbf{V}(\theta_k, \varphi_k) \cdot \mathbf{R} = \mathbf{V}_k \cdot \mathbf{R} \quad (4.7)$$

where

$$\mathbf{V}(\theta_k, \phi_k) = \begin{bmatrix} \cos \theta_k \cos \phi_k & \cos \theta_k \sin \phi_k & -\sin \theta_k \\ -\sin \phi_k & \cos \phi_k & 0 \\ \sin \theta_k \cos \phi_k & \sin \theta_k \sin \phi_k & \cos \theta_k \end{bmatrix} \quad (4.8)$$

Thus the value of this incident wave at a point  $\mathbf{R}$  in the unrotated frame is  $\tilde{\Psi}_c^{inc}(\mathbf{V}_k \cdot \mathbf{R})$ , but this is still a vector whose components are in the rotated frame. We map the vector components to the  $X, Y, Z$  frame by applying the inverse of the (orthogonal) rotation matrix:

$$\tilde{\Psi}^{inc}(\mathbf{R}) = \mathbf{V}_k^T \tilde{\Psi}_c^{inc}(\mathbf{V}_k \cdot \mathbf{R}) \quad (4.9)$$

Equation (4.12) represents a plane wave propagating in direction  $\theta_k, \phi_k$ , expressed in the  $X, Y, Z$  coordinate system.

Another polarization of this can be found by first rotating the canonical plane wave expression, Equation (4.7), by  $\phi = \pi/2$ . This rotated canonical wave is polarized along the  $Y$  axis but still propagates in the direction  $+Z$  as shown in Figure 4.9.

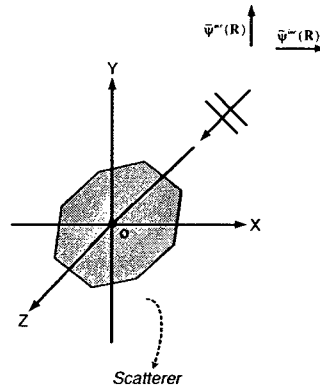


Figure 4.9 – A general single scatterer with an incident wave  $X$  or  $Y$  polarized propagating in the  $+Z$  direction.

Thus, following a similar procedure to that described above, we get

$$\tilde{\Psi}_c^{incY}(\mathbf{R}) = \mathbf{V}_Y^T \tilde{\Psi}_c^{inc}(\mathbf{V}_Y \cdot \mathbf{R}) \quad (4.10)$$

where

$$\mathbf{V}_Y = \mathbf{V}(0, \pi/2) \quad (4.11)$$

So, the complete set of incident waves is given by the following equations:

$$\tilde{\Psi}^{inc}(\mathbf{R}) = \mathbf{V}_k^T \tilde{\Psi}_c^{inc}(\mathbf{V}_k \cdot \mathbf{R}) \quad (4.12)$$

for  $X'$  - polarized plane waves

$$\tilde{\Psi}^{inc}(\mathbf{R}) = \mathbf{V}_k^T \tilde{\Psi}_c^{incY}(\mathbf{V}_k \cdot \mathbf{R}) \quad (4.13)$$

for  $Y'$  - polarized plane waves, where

$$\mathbf{V}_k = \mathbf{V}(\theta_k, \phi_k) \quad (4.14)$$

with  $k = 1, 2, \dots$  and

$$\tilde{\Psi}_c^{incY}(\mathbf{R}) = \mathbf{V}_Y^T \tilde{\Psi}_c^{inc}(\mathbf{V}_Y \cdot \mathbf{R}) \quad (4.15)$$

#### 4.2.2.2 STEP 2: Finding the scattered field

For each incident wave, the scattering problem must be solved in order to find the scattered field.

When the scatterer is spherically symmetric, the scattered field can be obtained for a given incident wave by rotation of the scattered field  $\tilde{\Psi}^{sca}$  derived for the canonical incident plane wave (Equation 4.5):

$$\tilde{\Psi}^{sca}(\mathbf{R}) = \mathbf{V}_k^T \tilde{\Psi}_c^{sca}(\mathbf{V}_k \cdot \mathbf{R}) \quad (4.16)$$

for  $X$  - polarized incident plane wave

$$\tilde{\Psi}^{sca}(\mathbf{R}) = \mathbf{V}_k^T \tilde{\Psi}_c^{scaY}(\mathbf{V}_k \cdot \mathbf{R}) \quad (4.17)$$

for  $Y$  - polarized incident plane wave, where

$$\mathbf{V}_k = \mathbf{V}(\theta_k, \phi_k) \quad (4.18)$$

$$\tilde{\Psi}_c^{scaY}(\mathbf{R}) = \mathbf{V}_Y^T \tilde{\Psi}_c^{sca}(\mathbf{V}_Y \cdot \mathbf{R}) \quad (4.19)$$

with  $k = 1, 2, \dots$

So, if the scatterer is spherically symmetric, the only field that has to be computed is for the canonical problem where the incident wave is an  $X$  polarized plane wave propagating in the  $+Z$  direction. All the others are found by rotation given by formula (4.19).

The canonical solution for the uniform dielectric sphere is given in Appendix A.

### 4.2.2.3 STEP 3: Mapping to the global coordinates

The last step consists of mapping the basis functions from  $X, Y, Z$  to the global coordinates  $x, y, z$ . This involves a translation and rotation. For the translation, first, we start with a point  $P = (x, y, z)$  as indicated in the Figure 4.10. Then, we find the coordinates  $x_c, y_c, z_c$  in a system based on the reference point of the scatterer, but parallel to  $x, y, z$ :

$$\mathbf{r}_c = \mathbf{r} - \mathbf{r}^j \quad (4.20)$$

where

$$\mathbf{r}_c = \begin{Bmatrix} x_c \\ y_c \\ z_c \end{Bmatrix}, \quad \mathbf{r} = \begin{Bmatrix} x \\ y \\ z \end{Bmatrix}, \quad \mathbf{r}^j = \begin{Bmatrix} x^j \\ y^j \\ z^j \end{Bmatrix} \quad (4.21)$$

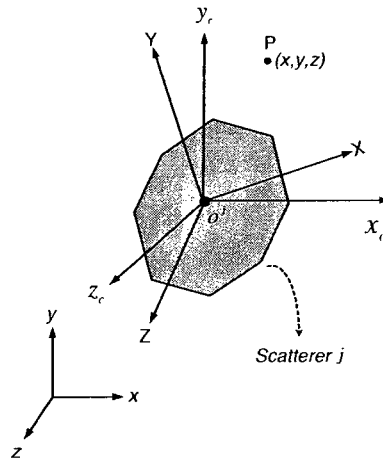


Figure 4.10 – Representation of the  $j^{\text{th}}$  scatterer with respect to a system.

Then, the coordinates with respect to the local frame can be obtained by applying a rotation, defined by two angles  $\theta^j$  and  $\varphi^j$  as shown in the Figures 4.11

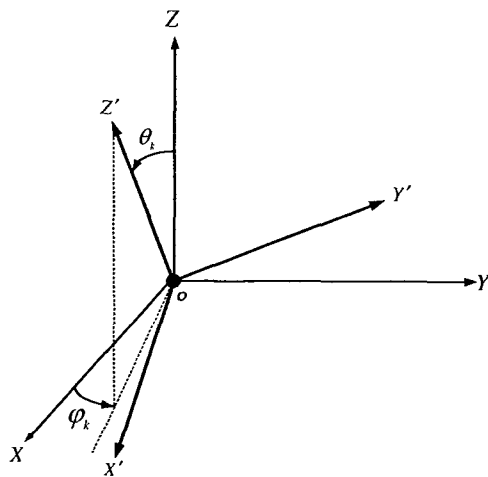


Figure 4.11 – Representation of both planar rotations:  $\varphi^j$  about Z axis and  $\theta^j$  about Y axis.

Finally, the overall effect of the translation and the rotations can be expressed by

$$\mathbf{R} = \mathbf{V}(\theta^j, \varphi^j) \cdot \mathbf{r}_c = \mathbf{V}^j \cdot (\mathbf{r} - \mathbf{r}^j) \quad (4.22)$$

Therefore, we can transform a vector basis function  $\tilde{\psi}(\mathbf{R})$  in the X, Y, Z frame of the  $j^{\text{th}}$  scatterer into

$$\psi(\mathbf{r}) = \mathbf{V}^{jT} \tilde{\psi}(\mathbf{V}^j \cdot (\mathbf{r} - \mathbf{r}^j)) \quad (4.23)$$

The right hand side of the Equation (4.23) is the value of the basis function at a global point  $\mathbf{r}$ . Thus, Equation (4.23) is what we need for the assembling of the FLAME molecule.

#### 4.2.3 Basis functions when there is no scatterer

This case can be derived from the previous one where there is a symmetric scatterer. When there is no scatterer, i.e. for the empty molecule,  $\mathbf{r}^j$  can be chosen anywhere and the basis functions are derived considering a complete set of plane waves defined by Equations (4.12) - (4.15).

### 4.3 ABC computational molecules

A scattering problem involves an unbounded domain, and so an artificial boundary is required as shown in Figure 4.12. Here, an absorbing boundary condition (ABC) is used that follows strictly the concept of the Trefftz - FLAME formulation. As a matter of fact, this ABC was already discussed in Chapter 2. The ABC in three dimensions is a straight forward extension of the one developed for the two dimensional problem. Thus, in order to define the ABCs, the basis functions are chosen to be plane waves that are biased in favor of outgoing waves. An artificial box is set around the computation domain as shown in Figure 4.12. We consider three types of boundary molecule: a half, a quarter and an eighth-molecule, as depicted in Figure 4.12. The Table 4.1 show the three types of ABC used and the number of basis functions for each type.

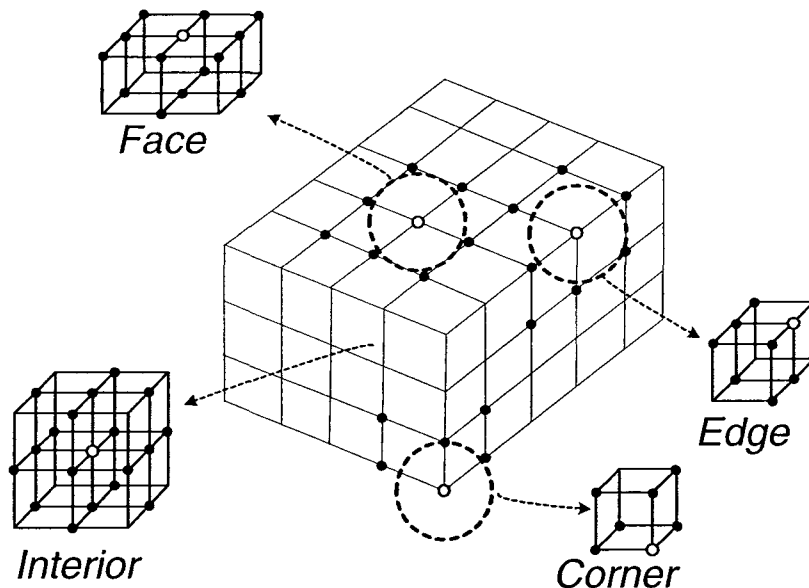


Figure 4.12 – The molecule for the interior nodes and the three types of molecule used at the boundaries where the ABC are set: A half, a quarter and an eighth-molecule. The open circle is the “centre” node of each molecule.

It is worth pointing out that this ABC is not geometric specific, i.e., the equations that define the molecules at the boundary are independent of the scatterer geometry.

TABLE 4.1– NUMBER OF BASIS FUNCTIONS FOR THE ABC-MOLECULE CONSIDERING ITS LOCATION ON AN ARTIFICIAL BOX SET AROUND THE COMPUTATION DOMAIN.

Molecule Size	Location	Number of Basis Functions, $m$	Number of non-centre nodes in the molecule, $n$
Full	Interior	36	18
Half	Faces	26	13
Quarter	Edges	18	9
Eighth	Corners	12	6

Each basis function is built from a corresponding incident plane wave, in exactly the same way as discussed in the previous section, for the interior molecule. There are two orthogonally - polarized plane waves for each direction. For the half - molecule, the 13 directions are formed by connecting the 13 non - centre nodes of the half-molecule with the “centre” node as shown in Figure 4.13. Following the same idea, the quarter (see Figure 4.14) and eighth-molecules (see Figure 4.15) utilize 9, and 6 directions, respectively.

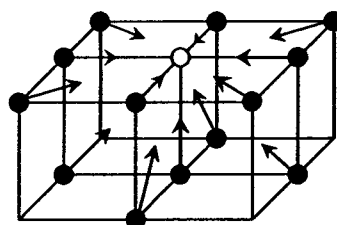


Figure 4.13 – Representation of a “face” molecule with 13 wave directions, one for each non-center node. The arrows indicate plane waves propagating along boundary or outwards only.

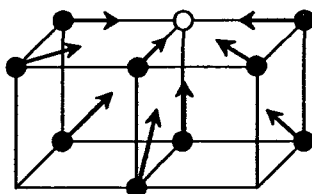


Figure 4.14 – Representation of a “edge” molecule with 9 wave directions, one for each non-center node.

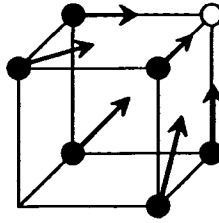


Figure 4.15 – Representation of a “corner” molecule with 6 wave directions, one for each non - center node.

#### 4.4 Setting the excitation – plane - ABC

As described in Chapter 3, the problem must be properly excited and reflections from the excitation plane placed at  $z = 0$ , must be absorbed. Therefore an excitation-plane- ABC must be imposed. Actually, it is set straightforwardly by adding the excitation function as indicated in the general FLAME molecule equation given by Equation (4.3). The right hand side of the Equations (4.3) is null for all interior molecules, for all ABC molecules except for those on the input plane. Thus, the Equation (4.3) is the general representation of Trefftz-FLAME for three dimensional problems, including the excitation-plane.

#### 4.5 Numerical experiments

##### 4.5.1 Single dielectric sphere

Consider a single dielectric sphere illuminated by a plane wave, Figure 4.16. The sphere has radius  $a = 0.25\lambda$  and relative permittivity  $\epsilon_r = 2$ . The surrounding free space is truncated by a square box, distance  $d/\lambda$  from the sphere. Here  $\lambda$  is the free-space wavelength.

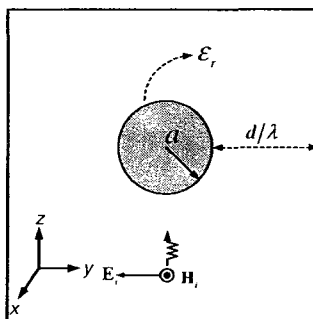


Figure 4.16 – A plane wave incident on a dielectric sphere with relative permittivity  $\epsilon_r$  and radius  $a$ .

Within the box, the new method is used with a grid spacing  $h$ . Figure 4.17 shows the RMS error in the computed electric field throughout the box, as a percentage of the amplitude of the field of the incident wave.

The RMS error is defined as

$$Error = \frac{1}{|\mathbf{E}^{inc}|} \sqrt{\frac{1}{N_p} \sum_{i=1}^{N_p} (\mathbf{E}_{ai} - \mathbf{E}_i)^2} \quad (4.24)$$

where  $\mathbf{E}_{ai}$  is the exact analytical solution given in appendix A by Equations (A.7) - (A.9) at a specific grid node, and  $\mathbf{E}_i$  is the FLAME solution obtained at the same node, and  $N_p$  represents the total number of nodes of the grid where the solution is evaluated. On the box surface, either the exact solution is enforced (stars in Figure 4.17), or an absorbing boundary condition (ABC) set at  $d/\lambda = 0.5$  (triangles) or  $d/\lambda = 1.5$  (squares) or  $d/\lambda = 2.5$  (circles). As can be seen, the error is less than 5% even when  $h/a = 1$ , when the sphere is just two grid cells across. When the exact solution is enforced (Dirichlet boundary condition) the error is less than 0.5% for  $h/a \leq 0.7$ . For the cases where ABCs are used, the errors are larger, as expected. By increasing  $d/\lambda = 0.5$  to  $d/\lambda = 2.5$  the errors are reduced, but there is no significant decrease of error when  $d/\lambda$  is increased from 1.5 to 2.5. In the ABC cases with  $d/\lambda > 0.5$ , the error is less than 1.5% for  $h/a \leq 0.7$ .

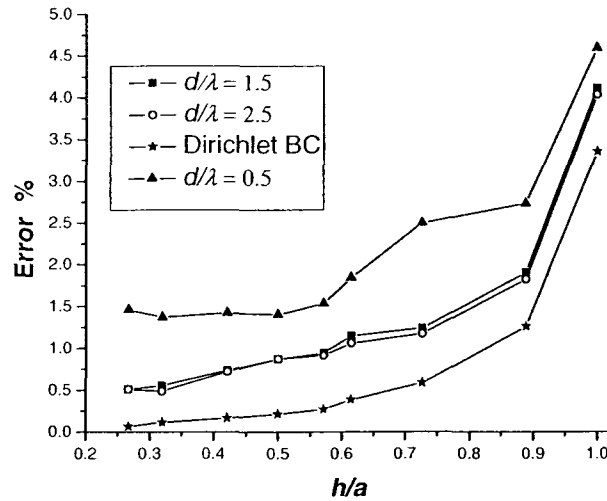


Figure 4.17 – The RMS errors versus grid spacing  $h/a$  for scattering from a single dielectric sphere are plotted for ABC set at  $d/\lambda=0.5$  (triangles),  $d/\lambda=1.5$  (squares) and  $d/\lambda=2.5$  (circles). The stars are the results when the Dirichlet boundary condition is imposed.

Thus, for the case considered, numerical experiments indicate that the ABC developed is a good radiation boundary condition when it is placed between  $0.5\lambda$  and  $1.5\lambda$  from the scatterers.

#### 4.5.2 Two spheres

To test the formulation for a system of spheres, we compared the FLAME results against previously published theoretical results [50] for the problem of light scattering from a chain of two spheres as indicated in Figure 4.18. The two spheres are identical with refractive index  $n_{sph} = 1.6 - 0.004j$  and radius  $a = 0.69\lambda$ . The centre-to-centre separation distance between the two spheres is  $s = 0.71\lambda$ . The surrounding free space is truncated by a rectangular box, distance  $d = 0.5\lambda$  from the spheres. Within the box, FLAME is used with  $h/a = 1/3$ .

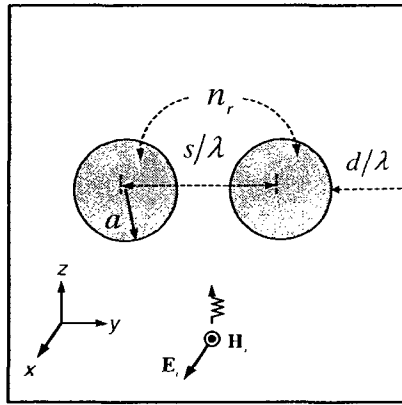


Figure 4.18 – Two identical lossy dielectric spheres.

The published results correspond to the scattered far field. However, Trefftz - FLAME computes directly the near field, so a near-to-far-field transformation was implemented [Appendix B] in order to compute the the normalized radar cross section (RCS) in the  $x - z$  plane ( $\phi = 0$ ) as a function of angle  $\theta$ . Specifically, the dimensionless quantity plotted is:

$$\frac{RCS}{\lambda^2} = \frac{4\pi r^2}{\lambda^2} \frac{|E_{\theta}^{sca}(r, \theta, \phi = 0)|^2}{|\mathbf{E}^{inc}|^2} \quad (4.25)$$

for  $r$  large enough that the point  $(r, \theta, 0)$  is in the far zone.

In Figure 4.19 RCS is plotted the as a function of angle  $\theta$  between the scattering direction and the  $z$  axis as defined by Equation (4.25). The results show a good agreement with Xu's theoretical results [50]. Thus, the method is validated for a multisphere problem.

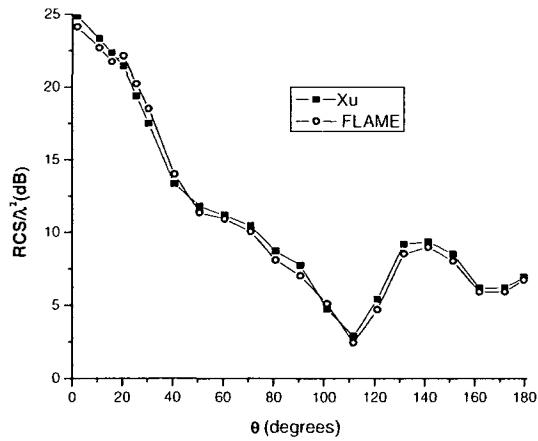


Figure 4.19 – RCS versus angle for the two-sphere problem. The “Xu” results are taken from [50].

### 4.5.3 A planar distribution of 10 dielectric spheres

As a final example, consider the array of 10 identical spheres shown in Fig. 4.20. Each sphere has a radius  $a=0.25\lambda$  and refractive index  $n_{sph}=1.5$ . The centers of the spheres all lie on  $z=0$ ; the normalized centre coordinates  $x_c/\lambda$  and  $y_c/\lambda$  are given in Table 4.2.

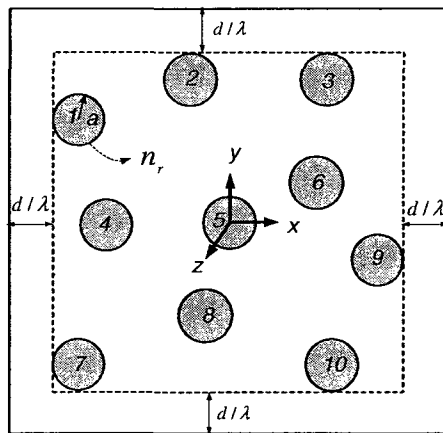


Figure 4.20 – A system of 10 dielectric spheres.

TABLE 4.2 – CENTRE COORDINATES  $x_c/\lambda$  ,  $y_c/\lambda$  FOR THE PLANAR DISTRIBUTION OF SPHERES REPRESENTED IN FIGURE 4.20.

Sphere number	$x_c/\lambda$	$y_c/\lambda$
1	-1.25	0.875
2	-0.1875	1.125
3	1.125	1.125
4	-1.125	-0.125
5	0	0
6	1.	0.125
7	-0.125	0.875
8	1.625	0.75
9	1.25	1.625
10	0.875	1.625

As in Fig. 4.20, an x-polarized incident plane wave propagates along the z axis towards the spheres, which are enclosed in a virtual boundary placed  $d = 0.75\lambda$  away. As before, the ABC molecules are used on the surface of the box. Fig. 4.21 shows the radar cross section (RCS) in the x - z plane ( $\phi = 0$ ) as a function of angle  $\theta$  between the scattering direction and the z axis.

There are no results from independent source available for this example, so instead it is analyzed by the new method with three different grid spacings:  $h/a = 2/3$ ,  $h/a = 1/2$  and  $h/a = 1/4$ . Assuming the last to be the most accurate, it can be seen that good accuracy is achieved even when  $h/a = 2/3$ , corresponding to just three grid cells across the diameter of the sphere. The peak difference between the  $h/a = 2/3$  and  $h/a = 1/4$  results occurs at  $\theta = 0$ , and is 0.6 dB. The average difference over the whole

range of  $\theta$  is 0.1 dB.

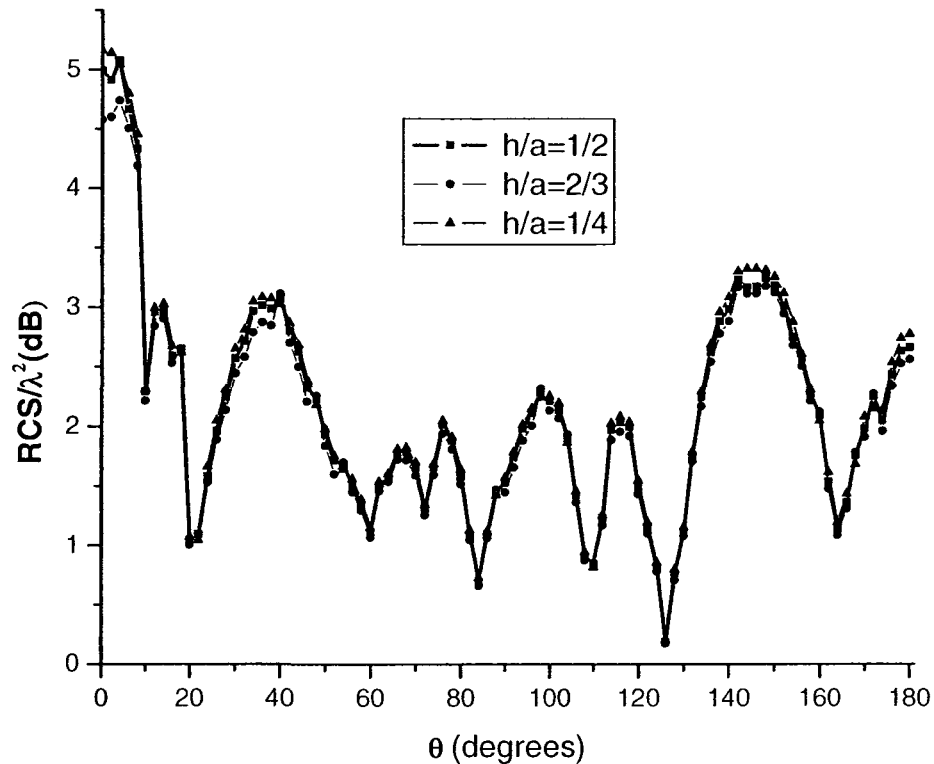


Figure 4.21 – Normalized RCS versus angle for the 10 spheres shown in Fig. 4.20.

#### 4.6 Conclusions

For the first time, a full vectorial Trefftz-FLAME method for three dimensional scattering is presented. It includes a formulation for both the interior domain and the boundary, where incident waves are excited and scattered waves are absorbed. Numerical experiments indicate that this ABC is effective when it is placed  $0.5\lambda$  or more from the scatterers. The efficiency of the formulation was shown by solving the problem of scattering from dielectric spheres. The FLAME results show good agreement with previously published values, both in the near field and the far field. Furthermore, the formulation presented is general and can be extended to non spherical scatterers by finding the local basis functions using numerical techniques, for instance FEM, instead of using the exact expressions available for the dielectric sphere.

## Chapter 5

### Conclusions

In essence, the objective of this work has been to develop an efficient, accurate and reliable method for the analysis of a problem containing a large number of repeated structures. To meet this goal a recently developed technique known as Trefftz-FLAME was enriched and expanded. First, the Trefftz-FLAME method for the analysis of PhC devices was presented. This included, for the first time, an eigenvalue analysis of the waveguide modes using FLAME. In addition, it was shown how the computed modes can be used to provide port boundary conditions for a PhC multiport device, and to extract reflection and scattering coefficients. The method was evaluated numerically for several PhC waveguides. The results matched well those obtained using currently available techniques such as FDTD, FEM and Plane Wave Expansion, but at lower computational cost.

In addition, the extension of Trefftz-FLAME to scattering of an electromagnetic wave by a number of identical, three-dimensional obstacles has been described. Conceptually this extension follows the previous two-dimensional formulation. Nevertheless, the problem was greatly increased by the need to develop new basis functions that satisfy the vectorial nature of the problem while at the same time avoiding ill-conditioning of the system matrix. In addition, a way of handling the boundaries of the three-dimensional computational domain was devised that absorbs outgoing waves and allows incident waves to be excited. Numerical simulations have proved that the three dimensional formulation can accurately model scattering from spheres that have fewer than four molecules across the diameter.

It is worth pointing out that Trefftz-FLAME schemes are not intended to replace general powerful tool such as FEM and FDM that are indispensable for modeling complex geometries. It has an advantage over these methods only when there are many similar structures present. In fact, the most promising development of this new technique is its integration with FEM or FDM, which could be used to find the local basis functions when there are no analytic solutions available for scattering from a single structure.

Trefftz-FLAME might be seen in future as a general framework that allows the cooperative work of many other numerical techniques acting to create local basis functions in a system containing a vast number of repeated structures with general shape and material composition.

## 5.1 Original contributions

In the course of developing Trefftz-FLAME in 2D, the following original contributions to knowledge have been made:

- a) Modal analysis based on Trefftz-FLAME for photonic crystals waveguides;
- b) Port boundary condition to properly excite the waveguide and absorb the reflections;
- c) Accurate calculation of transmission and reflection coefficients for several multi-port PhC waveguides;

With respect to 3D Trefftz-FLAME, the original contributions are:

- a) The first demonstration of FLAME for a 3D, vector problem of any kind;
- b) A general methodology for developing Trefftz-FLAME basis functions suitable for electromagnetic scattering from a number of identical obstacles;
- c) The development of molecules for the boundary of the computational domain, that allow for truncation of the vector field, both with respect to outgoing waves and the known incident wave.

## 5.2 Future trends

Several interesting opportunities for future studies should be noted. We can divide what could be done in three classes considering the level of difficulty for both mathematical development and implementation. First, for short term projects the following tasks could be accomplished:

- a) explore other lattice types for the PhC waveguide, e.g. waveguides created by either filling up or decreasing the sizes of the holes in triangular lattice for TM and TE-like waves [34, 35];

- b) analysis of Photonic Crystal Cavities [82, 83];
- c) analysis of Chain waveguides [84];
- d) combination of the 2D method with techniques that allow design optimization of PhC waveguides [85];
- e) development of new types of basis functions derived in closed form. For instance, basis functions that are the exact solution for the wave scattering problem from a multilayered [86], optically active chiral and chirally coated cylinders [87, 88];

Regarding the future trends of medium difficult, it is worth mentioning:

- a) development of new basis functions for the 3D-Trefftz-FLAME considering the exact solutions for the problem of wave scattering from a multilayered [89], chirally or optically active [90-92] and uniaxial anisotropic [93, 94] spheres;
- b) modal analysis to determine the photonic band gap for a three dimensional periodic array of dielectric spheres;
- c) introduction to the three dimensional formulation of the adaptive grid refinement method already developed for two dimensional formulations [39] .

Finally, the most demanding future work would be the development of basis functions by means of numerical techniques. In fact, this is the key to the future of Trefftz-FLAME. Efforts focusing on designing new basis functions might push away the limits of its applications. Local basis functions for nonspherical particles and particles composed of complex materials may be generated by well-established numerical techniques such as FEM [95] and FDTD [1]. Definitely, this would be not only the most interesting study but also an effective way of computing accurate near fields in many practical problems in three dimensions. This last line of study is likely to be both time consuming and mathematically demanding. However, the potential outcome of an efficient and reliable method for calculating the scattering of waves by nonspherical particles is both very important for a number of devices that could be in the next generation of devices for telecommunications, such as the ones based on 3D photonic crystals.

## Appendix A

### Basis functions for spherical dielectric scatterer

For the problem with a spherical dielectric scatterer, the basis functions are selected to be the canonical solution for the problem of scattering and absorption from a dielectric sphere excited by an arbitrary excitation as shown in the Figure A.1.

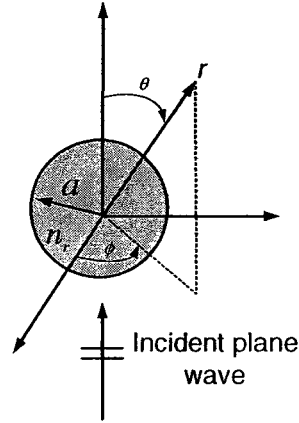


Figure A.1 – Spherical polar coordinate system centered on a spherical particle of radius  $a$  and refractive index  $n_s$ , is the refractive index for the exterior region and  $r$ ,  $\theta$  and  $\phi$  are the spherical coordinates.

The solution to this problem can be described by the following vector spherical harmonics:

$$\mathbf{M}_{emn} = \nabla \times (\mathbf{r} \times \psi_{emn}) \quad (\text{A.1})$$

$$\mathbf{M}_{omn} = \nabla \times (\mathbf{r} \times \psi_{omn}) \quad (\text{A.2})$$

$$\mathbf{N}_{emn} = \frac{\nabla \times \mathbf{M}_{emn}}{k} \quad (\text{A.3})$$

$$\mathbf{N}_{omn} = \frac{\nabla \times \mathbf{M}_{omn}}{k} \quad (\text{A.4})$$

where subscripts  $e$  and  $o$  denotes even and odd,  $\psi_{emn}$  and  $\psi_{omn}$  are generating functions that satisfy the scalar wave equation in spherical coordinate:

$$\psi_{emn} = \cos m\phi P_n^m(\cos \theta) z_n(kr) \quad (\text{A.5})$$

$$\psi_{omn} = \sin m\phi P_n^m(\cos\theta)z_n(kr) \quad (\text{A.6})$$

where  $z_n$  is any of the three spherical Bessel function:  $j_n, h_n^{(1)},$  or  $h_n^{(2)}$  which represent the standing, inward - traveling and outward - traveling waves, respectively. The function  $P_n^m$  is the Associated Legendre function [73 - 75], and  $k$  is the wavenumber for the medium. The problem described above is a classical problem where Mie - theory is applied, see details in [61 - 63, 75]. Using the vector spherical harmonics defined by Equations (A.1) - (A.3), the following expansions are derived for the fields:

$$\mathbf{E}^{Inc}(\mathbf{r}, \theta, \phi) = -E_0 \sum_{n=1}^{\infty} j^n \frac{(2n+1)}{n(n+1)} (\mathbf{M}_{o1n}^{(1)} + j\mathbf{N}_{e1n}^{(1)}) \quad (\text{A.7})$$

$$\mathbf{E}^{Sca}(\mathbf{r}, \theta, \phi) = -E_0 \sum_{n=1}^{\infty} (a_n \mathbf{M}_{o1n}^{(3)} + jb_n \mathbf{N}_{e1n}^{(3)}) \quad (\text{A.8})$$

$$\mathbf{E}^{Inter}(\mathbf{r}, \theta, \phi) = -E_0 \sum_{n=1}^{\infty} (c_n \mathbf{M}_{o1n}^{(1)} + jd_n \mathbf{N}_{e1n}^{(1)}) \quad (\text{A.9})$$

here,  $\mathbf{E}^{Inc}$ ,  $\mathbf{E}^{Sca}$  and  $\mathbf{E}^{Inter}$  are the incident, scattered and internal fields, respectively, The coefficients  $a_n$ ,  $b_n$  are used to compute the amplitudes of the scattered field, and  $c_n$  and  $d_n$  are used to compute the amplitudes of the internal field, respectively [62, 63]. We append (A.1), (A.2) and (A.3) to the vector spherical harmonic for which the radial dependence of generating functions is specified by  $j_n, h_n^{(2)}$  and  $h_n^{(1)}$ , respectively. It is worth pointing out that  $\mathbf{M}_{o1n}$  and  $\mathbf{N}_{e1n}$  represent TM and TE waves, respectively. Therefore, applying the boundaries conditions at  $r = a$ , two decoupled equations are derived and solved separated for the scattering coefficients ( $a_n, b_n$ ) and internal coefficients ( $c_n, d_n$ ). These Mie coefficients were evaluated using MATLAB's built-in double precision Bessel functions [76].

As indicated by the problem statement, the expressions (A.7) - (A.9) were derived for  $X$  - polarized incident plane wave. Even so, the derivation of scattering and internal fields for  $Y$  - polarized incident plane waves can be easily determined using the following equivalency

$$\mathbf{E}(\phi; x - polarized) = \mathbf{E}(\phi + \frac{\pi}{2}; y - polarized) \quad (\text{A.10})$$

Moreover, the number of terms for the field expansions is normally chosen to be proportional to the size parameter of the sphere defined as

$$x_{size} = (2\pi/\lambda)n_{sph}a \quad (\text{A.11})$$

The criterion developed by Wiscombe [77] and modified by Bohren and Hoffman [62] provides a good estimative of required number of terms  $n$ . This criterion is given as

$$N_{Terms} \approx x_{size} + 4x_{size}^{1/3} + 2 \quad (\text{A.12})$$

Thus, for the computation molecule overlapping a dielectric sphere, the basis functions are derived from equations (A.7) - (A.10) when planes waves of different directions scatter from the sphere.

## Appendix B

### Far field calculations

To calculate the scattered far field, either a surface or a volume integration approach can be exploited. Here the former was adopted, by enclosing the scatterers by a surface, an imaginary box located between the scatterers and the outer boundary (where the ABC is applied). Then, the far field is computed by carrying out the integration over the surface. An informative and detailed derivation of the far field is given in [1, 61, 80].

According to the equivalence theorem, the far field can be computed if the tangential components of the electric and magnetic fields on the surface of the scattering particle are known [79] (Jackson, 1998, p. 485):

$$\mathbf{E}^{scat}(\mathbf{r})\Big|_{kr \rightarrow \infty} = \frac{jk \exp(-jkr)}{4\pi r} \int_{S'} \mathbf{Z} \times \exp(jk\mathbf{n}\cdot\mathbf{r}') dS' \quad (\text{B.1})$$

where

$$\mathbf{Z} = \mathbf{r}' \times \{ \mathbf{J}_s(\mathbf{r}') - \mathbf{M}_s(\mathbf{r}') \} \quad (\text{B.2})$$

The vectors  $\mathbf{J}_s(\mathbf{r}') = \hat{\mathbf{n}}_s \times \mathbf{E}(\mathbf{r}')$ ,  $\mathbf{M}_s(\mathbf{r}') = \hat{\mathbf{n}}_s \times \mathbf{H}(\mathbf{r}')$  are the equivalent electric and magnetic currents that replace the scatterer and  $\hat{\mathbf{n}}_s$  is an outward-pointing unit vector normal to the surface  $S'$  as indicated in Figure B.1. Equation (B.1) shows that one can determine the far-field by weighting the near-field with the free-space Green's functions and integrating it over a surface  $S'$  surrounding the scatters. In the far field, that is  $kr \rightarrow \infty$ ,  $\hat{\mathbf{r}} \cdot \mathbf{E}^{scat}(\mathbf{r}) = 0$ .

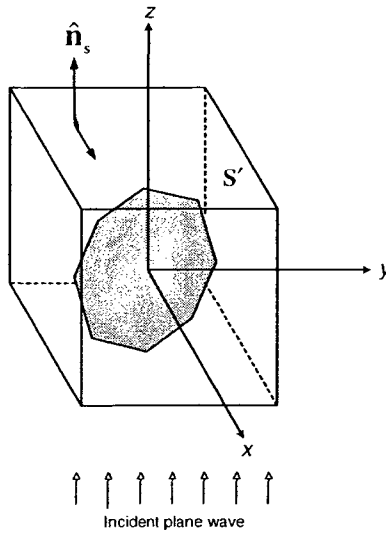


Figure B.1 – Representation of the surface of integration for computing the near to far field transformation.

In summary, first FLAME - Trefftz is used to compute the near - field  $\mathbf{E}(\mathbf{r}')$  in and around the scatterers. Then, the coefficients  $c_k$  are computed as

$$\{c\} = [\mathbf{Q}] \cdot (\{\mathbf{E}\} - \{\mathbf{E}^{inc}\}) \quad (B.3)$$

Afterwards, using equation (4.3) of Chapter 4, we can obtain the magnetic field as

$$\mathbf{h}(\mathbf{r}) = -\sum_{k=1}^m \left( \frac{c_k \nabla \times \Psi_k + \nabla \times E^{inc}(\mathbf{r})}{j\omega\mu} \right)_k \quad (B.4)$$

where  $\omega$  is the angular frequency and  $\mu$  is the permeability of the medium. The equation (B.4) is needed to calculate  $Z$  given by Equation B.2. Finally, using Equation B.1, the normalized radar cross section (RCS) in the x-z plane ( $\phi = 0$ ) is computed as

$$\frac{RCS}{\lambda^2} = \frac{4\pi r^2 |E_{\theta}^{scd}(r, \theta, \phi = 0)|^2}{\lambda^2 |\mathbf{E}^{inc}|^2} \quad (B.5)$$

Here  $\theta$  is the angle between the scattering direction and the z axis.

Equation (B.1) are solved by applying double integration molecule for Simpson's 1/3 rule [81] to a surface  $S'$  made up of the six plane surfaces of a box, shown in Figure 1. The corresponding schematic or integration molecule is shown in Figure B.2.

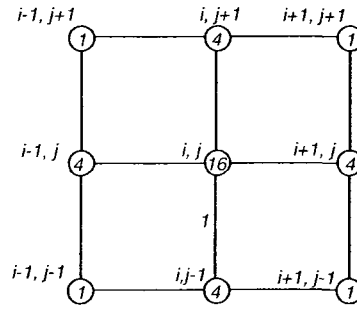


Figure B.2 – Double Integration molecule for Simpson's 1/3 rule.

In the Figure B.2,  $i, j$  is a grid node that belongs to the surface  $S'$ . By applying the Simpson's 1/3 rule one gets the following expression for a sub area:

$$A_{ij} = \frac{h^2}{9} [(f_{i+1,j+1} + f_{i+1,j-1} + f_{i-1,j+1} + f_{i-1,j-1}) + 4(f_{i,j+1} + f_{i,j-1} + f_{i+1,j} + f_{i-1,j}) + 16f_{i,j}] \quad (\text{B.6})$$

## References

- [1] Taflove, A. and Hagness, S. C., Computational electrodynamics: The finite-difference time-domain method, 3rd ed., Artech House , Boston, MA, 2005.
- [2] Guoqiang Shen, Cange Ilaris, A.C , “A new FDTD stencil for reduced numerical anisotropy in the computer modeling of wave phenomena”, International Journal of RF and Microwave Computer-Aided Engineering, Vol 17, No 5, pp 447-54, September 2007.
- [3] Capoglu, I.R ,Smith, G.S, A total-field/scattered-field plane-wave source for the FDTD analysis of layered , IEEE Transactions on Antennas and Propagation, Vol 56, No 1, pp 158-69, January 2008.
- [4] D Degerfeldt, David and Rylander, Thomas (2008) 'Scattering Analysis by a Stable Hybridization of the Finite Element Method and the Finite-Difference Time-Domain Scheme with a Brick-Tetrahedron Interface', Electromagnetics, Vol 28, pp. 3 - 17 May 2008.
- [5] C. Mias, J. P. Webb, L. El-Esber, and R. L. Ferrari, "Finite element modelling of electromagnetic waves in doubly and triply periodic structures," IEE Proceedings-Optoelectronics, Vol. 152, pp. 274-274, October 2005.
- [6] Y. Cai and C. Mias, "Fast finite element time domain - Floquet modal absorbing boundary condition modelling of periodic structures using recursive convolution," IEEE Transactions on Antennas and Propagation, Vol. 55, pp 2550-2558, September 2007.
- [7] Petersson, L.E.R. , Jian-Ming Jin, “Three-dimensional time-domain finite-element formulation for periodic structures”, IEEE Transactions on Antennas and Propagation, Vol 54, No 1, pp 12-19, January 2006.
- [8] Petersson, L.E.R., Jian-Ming Jin, “Analysis of periodic structures via a time-domain finite-element formulation with a Floquet ABC”, IEEE Transactions on Antennas and Propagation, Vol 54, No 3, pp 933-44, March 2006.

- [9] Marinos N. Vouvakis, Zoltan Cendes, and Jin-Fa Lee, "A FEM Domain Decomposition Method for Photonic and Electromagnetic Band Gap Structures", IEEE Transactions Antennas and Propagation, Vol. 54, No. 2, February 2006.
- [10] I. Tkukerman, "A Flexible Approximation Method for Electro and Magnetostatics," IEEE Transactions Magnetics, Vol. 40, No. 2, pp. 941-944, March 2004.
- [11] I. Tsukerman, "Electromagnetic applications of a new finite-difference calculus", IEEE Transactions Magnetics, Vol. 41, No. 7, pp. 2206-2225, July 2005.
- [12] Trefftz, "Ein Gegenstück zum Ritzschen Verfahren," In: 2. Int. Kongr. für Techn. Mech., Zürich, pp. 131–137, 1926.
- [13] J. Jirousek and A. P. ZielinÂski, "Survey of Trefftz-Type Element Formulations", Computers and Structures, Vol. 63, No. 2, pp. 225-242, April 1997.
- [14] R. Piltner, "Recent developments in the Trefftz method for finite element and boundary element applications", Advances in Engineering Software, Vol. 24, pp. 107-115, 1995.
- [15] Qing-Huan Qin, "Trefftz Finite Element Method and its Applications", Transactions ASME, Vol.58, pp. 316-337 ,September 2005.
- [16] J. T. Chen, C. S. Wu, Y. T. Lee, "On the equivalence of the Trefftz method and method of fundamental solutions for Laplace and biharmonic equations", Computers and Mathematics with Applications, Vol.53, pp. 851-879, March 2007.
- [17] B. Pluymers, B. van Hal, D. Vandepitte, W. Desmet, "Trefftz-Based Methods for Time- Harmonic Acoustics," Archives of Computational Methods in Engineering , Vol. 14, No 4, pp. 343-381, December 2007.
- [18] Olgierd C. Zienkiewicz, "Trefftz type approximation and the generalized finite element method – history and development", Computer Assisted and Engineering Sciences, pp. 305-316, 1997.
- [19] W. Yeih, R. F. Liu, J. R. Chang, and S. R. Kuo, "Numerical instability of the direct Trefftz method for Laplace problems in a 2D finite domain", The International Journal of Applied Mathematics and Mechanics (IJAMM), Vol. 2, pp. 41-66, 2006.
- [20] W. G. Jin, "Trefftz direct method", Advances in Engineering Software, Vol 24, Issues 1-3, pp. 65-69, 1995.

- [21] Miklos Gyimesi, Igor Tsukerman and Doug Lavers, "Hybrid Finite Element – Trefftz Method for Open Boundary Analysis," IEEE Transactions on Magnetics, Vol. 32, No. 3, pp. 671-674, May 1996.
- [22] T. Omuki, S. Wakao, T. Kuwahara, and Jee-Won Im, "Hybrid Trefftz and Finite Element Method Applied to Magnetic Analysis for Rotating Machines", IEEE Transactions on Magnetics, Vol. 32, No. 2, pp. 2014-2017, March 1997.
- [23] A. P. Zielinski, Q. C. Zienkiewicz, "Generalized Finite Element Analysis With T-Complete Boundary Solution Functions," International Journal for Numerical Methods in Engineering, Vol. 21, pp. 509–528, 1985.
- [24] Ismael Herrera, "Trefftz Method: A General Theory", Numerical Methods for Partial Differential Equations, Vol. 16, Issue 6, p. 561-580, October 2000.
- [25] L. Proekt, S. Yuferev, I. Tsukerman, and N. Ida, "Method of overlapping patches for electromagnetic computation near imperfectly conducting cusps and edges," IEEE Transactions on Magnetics, Vol. 38, pp. 649-652, Mar 2002.
- [26] Yury Olgovich Shlepnev, "Trefftz Finite Elements for Electromagnetics," IEEE Journal of Light Technology, Vol. 50, No. 5, pp. 1328-1339, May 2002.
- [27] K. Sakai, "Locally Exact Numerical Scheme with nonoscillation properties for stationary Transport Equations with absorption and Source Terms," Nuclear Science and Engineering, Vol. 123, No. 1, pp. 57-67, May 1996.
- [28] G. Ronald Hadley, "High-accuracy finite-difference equations for dielectric waveguide analysis I: uniform regions and dielectric interfaces", Journal of Light Technology, Vol. 20, Issue 7, Page 1210-1218, Jul. 2002.
- [29] G. Ronald Hardley, "High - Accuracy finite - difference equations for dielectric waveguide analysis II: dielectric corners", IEEE Journal of Lightwave Technology, Vol. 20, No. 7, pp. 1219-1231, 2002.
- [30] G. Ronald Hardley, "Low-Truncation-Error Finite Difference Equations for Photonics Simulation II: Vertical-Cavity Surface-Emitting Lasers," IEEE Journal of Lightwave Technology, Vol. 16, No. 1, pp. 142-151, January 1998.
- [31] Igor Tsukerman, "A new FD calculus: simple grids for complex problems", The International Compumag Society Newsletter, Vol. 12, No. 2, pp. 3–17, July 2005.

- [32] Igor Tsukerman, “A class of difference schemes with flexible local approximation,” The Journal of Computational Physics, Vol. 211, No. 2, pp. 659–699, January 2006.
- [33] I. Tsukerman, private communication, 2004.
- [34] J. Dai, I. Tsukerman, A. Rubinstein, S. Sherman, “New computational models for electrostatics of macromolecules in solvents”, IEEE Transaction on Magnetics, Vol. 43, No. 4, pp.1217–1220, April 2007.
- [35] Igor Tsukerman, “Electromagnetic finite-difference analysis without the ‘staircase’ effect,” 2005 IEEE/ACES International Conference on Wireless Communications and Applied Computational Electromagnetics, Honolulu HI, April 2005.
- [36] Jianhua Dai, Igor Tsukerman, “Difference Schemes with Local Numerical Bases for Multiparticle Interactions,” Twelfth Biennial IEEE Conference on Electromagnetic Field Computation (CEFC 2006), Miami, FL, April 30 – May 3, 2006.
- [37] Friedman, G. Yellen, B. Tsukerman, I., “Design and simulation of magnetically controlled nanoscale assembly”, Conference on Nanotechnology 4th IEEE, pp. 56-58, August 2004.
- [38] Masha Sosonkina and Igor Tsukerman, “Parallel solvers for flexible approximation schemes in multiparticle simulation”, ICCS 2006: Advancing Science through Computation, University of Reading, UK, May 28–31, 2006.
- [39] Jianhua Dai, Igor Tsukerman, “Flexible approximation schemes with adaptive grid refinement”, Compumag’2007, Aachen, Germany, June 2007.
- [40] Igor Tsukerman, “A new computational method for plasmon resonances of nanoparticles,” 2005 IEEE/ACES International Conference on Wireless Communications and Applied Computational Electromagnetics, Honolulu HI, April 2005.
- [41] František Čajko and Igor Tsukerman, “New methods and application in nanophotonics,” Compumag’2007, Aachen, Germany, June 2007.
- [42] František Čajko and Igor Tsukerman, “Flexible approximation schemes for wave refraction negative index materials,” Compumag’2007, Aachen, Germany, June 2007.

- [43] J. D. Joannopoulos, R. D. Meade, and J. N. Winn, Photonic Crystals: Molding the Flow of Light, Princeton: Princeton University Press, 1995.
- [44] Jonhson S. G. and Joannopoulos J. D., Photonic Crystals: The Road from Theory to Practice, Boston:Kluwer, 2002.
- [45] H. F. Pinheiro, J. P. Webb, I. Tsukerman, "Scattering in photonic crystal devices using the Flexible Local Approximation Method", Twelfth Biennial IEEE Conference on Electromagnetic Field Computation (CEFC 2006), Miami, FL, April 30 – May 3, 2006.
- [46] H. F. Pinheiro, J. P. Webb, I. Tsukerman, "Flexible local approximation models for wave scattering in photonic crystal devices," IEEE Transactions on Magnetics, Vol. 43, No. 4, pp. 1321–1324, 2007.
- [47] Leung Tsang, Jin Au Kong, Kung-Hau Ding, Chi On Ao, Scattering of Electromagnetic Waves: Numerical Simulations, John Wiley & Sons, Inc. 2002.
- [48] Michael I. Mishchenko, Joop W. Hovenier, and Larry D. Travis, Light Scattering by Nonspherical Particles, Academic Press, 2000.
- [49] Andrew Dunn and Rebecca Richards-Kortum, "Three-Dimensional Computational of Light Scattering From Cells," IEEE Journal of Selected Topics in Quantum Electronics, Vol. 2, No. 4, December 1996.
- [50] Yu-lin Xu, "Electromagnetic scattering by an aggregate of spheres," Applied Optics, Vol. 34, No. 21, pp. 4573–4588, 20 July 1995 .
- [51] Yu-lin Xu, "Electromagnetic scattering by an aggregate of spheres: far field," Applied Optics, Vol. 36, No. 36, pp. 9496-9508, 20 December 1997.
- [52] Y. -L. Xu, and Bo Å. S. Gustafson, "Comparison between Multisphere Light-scattering Calculations: Rigorous Solution and Discrete Dipole Approximation," The Astrophysical Journal, pp. 894-909, 1999.
- [53] Y.-L. Xu, "Electromagnetic scattering by an aggregate of spheres: theoretical and experimental study of the amplitude scattering matrix," Physics Review E, Vol. 58, No. 3, pp. 3931-3948, September 1998.
- [54] Y.-L. Xu, and Bo Å. S. Gustafson, "Experimental and theoretical results of light scattering by aggregates of spheres", Applied Optics, Vol. 36, No. 30, pp. 8026-8030, 20 October 1997.

- [55] H. Chew, D. D. Cooke, and M. Kerker, "Raman and fluorescent scattering by molecules embedded in concentric sphere," Journal of the Optical Society of America, Vol. 66, No. 5, pp. 440-444, May 1976.
- [56] P. W. Dusel, M. Kerker, and D. D. Cooke, "Distribution of Absorption Centers Within Irradiated Spheres," Journal of the Optical Society of America, Vol. 69, No. 1, pp. 55-59, January 1979.
- [57] Alfons Hoekstra, Jussi Rahola, and Peter Sloot, "Accuracy of Internal Fields in Volume Integral Equation Simulations of Light Scattering", Applied Optics, Vol. 37, No. 36, pp.8482-8497, December 1998.
- [58] [Changhui Li, George W. Kattawar, Peng-Wang Zhai, Ping Yang, "Electric and magnetic energy density distributions inside and outside dielectric particles illuminated by a plane electromagnetic wave", Optical Express, Vol.13, No.12, pp. 4554-4559, 13 June 2005.
- [59] E. Flück, N. F. van Hulst,, W. L. Vos, and L. Kuipers, "Near-field optical investigation of three-dimensional photonic crystals," Physics Review E 68, pp. 1-4, 2003.
- [60] Y. Tsuji, M. Koshiba, "Finite element method using port truncation by perfectly matched layer boundary conditions for optical waveguide discontinuity problems," IEEE Journal of Lightwave Technology, Vol. 20, No. 3, pp.463-468.
- [61] Constantine A. Balanis, Advanced Engineering Electromagnetic, John Wiley & Sons, 1989.
- [62] C. F. Bohren and D. R. Huffman, Absorption and Scattering of Light by Small Particles, Wiley, New York, 1983.
- [63] H. C. Van de Hulst, Light Scattering by Small Particles, Dover, New York, 1981.
- [64] A. Mekis, J. C. Chen, I. Kurland, S. Fan, R. Villeneuve, and J. D. Joannopoulos, "High transmission through sharp bends in photonic crystal waveguides", Physics Review Letter, Vol. 114, pp. 185-200, Oct. 1994.
- [65] M. Koshiba, Y. Tsuji, and M. Hikari "Time-Domain Beam Propagation Method and Its Application to Photonic Crystal Circuits,"IEEE Journal of Lightwave Technology, Vol. 18, No. 1, pp. 102-110, January 2000.

- [66] S. Fan, S. G. Johnson, and J. D. Joannopoulos, "Waveguide branches in photonic crystals," Journal of the Optical Society of America B, Vol. 18, No. 2, Feb. 2001.
- [67] A. Matsushima, Y. Momoka, M. Ohtsu, and Y. Okuno, "Efficient Numerical Approach to Electromagnetic Scattering from Three-Dimensional Periodic Array of Dielectric Spheres Using Sequential Accumulation," Progress in Electromagnetics, PIER, pp. 305-322, 2007.
- [68] Hong-Xing Xu, "A new method extending Mie theory to calculate local field in outside/inside of aggregates of arbitrary spheres", Physics Letters A, pp. 411-419, 2003.
- [69] Hongxing Xu, "Calculation of the near field of aggregates of arbitrary spheres", Journal Optical Society of America, pp. 804-808, Vol. 21, No. 5, May 2004.
- [70] Murili M. Gupta and Jules Kouatchou, "Symbolic Derivation of Finite Difference Approximations for the Three-Dimensional Poisson Equation", Numerical Methods for Partial Differential Equations, Vol. 14, Issue 5, pp. 593-606, 1998.
- [71] R. Steijl, H. W. M. Hoeijmakers, "Fourth-order accurate compact-difference discretization method for Helmholtz and incompressible Navier-Stokes equations", International Journal for Numerical Methods in Fluids, 46, pp. 227-244, 2004.
- [72] Lothar Collatz, The Numerical Treatment of Differential Equations, New York:Springer, 1966.
- [73] Shanjie Zhang, Jianning Jin, Computation of Special Functions, Wiley Interscience, 1996.
- [74] Abramowitz, Handbook of Mathematical Functions, Dover Publications, 1972.
- [75] Roger F. Harrington, Time-Harmonic Electromagnetic Fields, Wiley- IEEE Press; 2nd edition, 2001.
- [76] Math Works, MATLAB User's Guide, The Mathworks Inc., Natick, MA, 1992.
- [77] W. J. Wiscombe, "Improved Mie Scattering algorithms", Applied Optics, Vol. 19, pp. 1505-1509, May 1980.
- [78] Chen-To Tai, Generalized Vector and Dyadic Analysis Applied Mathematics in Field Theory, IEEE Computer Society Press, 1997.

- [79] J. D. Jackson, Classical Electrodynamics, Second edition, John Wiley and Sons, New York, 1975.
- [80] Allen Taflove, Korada Umashankar, "Radar Cross Section of General Three-Dimensional Scatterers", IEEE Transactions on Electromagnetic Compatibility, Vol. EMC 25, No. 4, pp. 433-440, November 1983.
- [81] Matthew N. O. Sadiku, Numerical Techniques in Electromagnetics, 2001.
- [82] Guo Qin Huang, Application of the Flexible Local Approximation Method to Photonic Crystal Cavities, Master Thesis, McGill, 2006.
- [83] Huanhuan Gu, Photonic Crystal Cavity Analysis Using a Simplified Flexible Local Approximation Method with an Anisotropic Perfectly Matched Layer Boundary Condition, Master thesis, McGill, 2006.
- [84] Pi-Gang Luan, Kao-Der Chang, "Transmission Characteristics of Finite Periodic Dielectric Waveguides", Optics Express, Vol. 14, No. 8, pp.3263-3272, February 2006.
- [85] Jasmin Smajic, Christian Hafner, and Daniel Erni, "Optimization of Photonic Crystal Structures", Optical Society of America, Vol. 21, No. 11, pp. 2223-2232, November 2004.
- [86] Renxian Li, Xiang'e Han, Huifen Jiang, and Kuan Fang Ren, "Debye Series of Normally Incident Plane-Wave Scattering by an Infinite Multilayered Cylinder", Applied Optics, Vol. 45, No. 24, pp. 6255-6262, August 2006.
- [87] Craig F. Bohren, "Scattering of Electromagnetic Waves by an Optically Active Cylinder", Journal of Colloid and Interface Science, Vol. 66, No. 1, pp. 105-109, August, 1978.
- [88] Reena Sharma and Balakrishnan, "Scattering of electromagnetic waves from chirally Coated Cylinders," Smart Materials and Structures, 7, pp. 512-521, 1998.
- [89] Weng Yang, "Improved Recursive Algorithm for Light Scattering by a multilayered Sphere", Applied Optics, Vol. 42, No. 9, pp. 1710-1719, March 2003.
- [90] Craig F. Bohren, "Light Scattering by an Optically Active Sphere", Chemical Physics Letter, Vol. 29, No. 3, pp. 458-462, December 1974.

- [91] Craig F. Bohren, "Scattering of Electromagnetic Waves by an Optically Active Spherical Shell, The journal of Chemical Physics, Vol. 62, No. 4, pp. 1566-1571.
- [92] Veysel Demir, Atef Elsherbeni, Denchai Worasawate, and Ercument Arvas, "A Graphical User Interface (GUI) for Plane-Wave Scattering from a Conducting, Dielectric, or Chiral Sphere," IEEE Antennas and Propagation Magazine, Vol. 46, No. 5, 94-99, October 2004.
- [93] Cheng-Wei Qui, Le-Wei, and Tat-Soon Yeo, "Scattering by rotationally symmetric anisotropic spheres: Potential formulation and parametric studies", Physical Review E, 75, pp. 1-8, 2007.
- [94] K. L. Wong and H. T. Chen, "Electromagnetic scattering by a uniaxially anisotropic sphere", IEE Proceedings-H, Vol. 139, No. August 1992.
- [95] Jin, J. , The Finite Element Method in Electromagnetics, J. Wiley & Sons, New York, 1993.